Parameter estimation

Oliwer **Sliczniuk**^{*a,*}, Pekka **Oinas**^{a}

^{a}*Aalto University, School of Chemical Engineering, Espoo, 02150, Finland*

ARTICLE INFO

ABSTRACT

This study aimed to investigate the supercritical extraction process of the caraway oil from caraway seeds from a partially filled extractor with a fixed bed operated under multiple constant operating conditions. The dataset collected from the experiments consists of four experiments conducted at different operating conditions: $40°C/200$ bar, $50°C/200$ bar, $40°C/300$ bar, and $50°C/300$ bar. A distributed-parameter model is used to describe the fluid-solid extraction process with CO_2 as a solvent. The concept of quasi-one-dimensional flow is applied to reduce the number of spatial dimensions. The flow is assumed to be uniform across any cross-section, although the area available for the fluid phase can vary along the extractor. This model requires parameters such as partition factor, internal diffusion coefficient, axial diffusion coefficient, saturation concentration, and an initial state estimate. These parameters are estimated from the Peng-Robinson equation of state and by applying the maximum likelihood estimation method on yield data under the normal error assumption.

1. Introduction

The present study focuses on extracting essential oil from the caraway (Carum carvi L.) seeds with supercritical fluid extraction and modelling that process. Caraway is a biennial plant belonging to the Apiaceae family. It is widespread in Asia, Europe, and North Africa. The essential oil obtained from caraway finds its potential application as a fragrance ingredient in perfumes, liquors, and toothpaste. As presented by Hromis et al. [1], the dried caraway contains nearly 2.8–5% essential oil, from which the main compounds are carvone, pinene, camphene, limonene, and carveol.

The economic feasibility of the process is crucial when selecting the appropriate technology. Conventional processes, such as distillation and organic solvent extraction, are frequently used for essential oil extraction. The distillation process is carried out at a high temperature, which causes thermal degradation of thermolabile compounds—considering that alternative techniques like supercritical fluid extraction gained popularity for extraction. Supercritical CO_2, in particular, is attractive due to its unique properties such as inflammable, non-toxic, low critical temperature and non-corrosive. Furthermore, its critical point is relatively low compared to other fluids, making it a suitable alternative to traditional extraction techniques. The supercritical fluids exhibit both gas- and liquid-like properties so that operating conditions can adjust pressure-depended dissolving power.

Various mathematical models have been proposed to describe the extraction of valuable compounds from a fixed biomass bed. However, selecting an appropriate extraction model requires understanding the physical phenomena occurring in the operational unit. Each model has its own set of assumptions and describes different mass transfer mechanisms and equilibrium relationships.

One model proposed by Reverchon et al. [2] is the hot ball model, which is based on an analogy to heat transfer and describes an extraction process from solid particles containing small quantities of solute where solubility is not a limiting factor. Another model, the Broken-and-Intact Cell model, was presented by Sovova [3]. This model describes a system where the outer surfaces of particles have been mechanically interrupted, allowing easy access of solvent to the solute from the broken cells. In contrast, the solute from the intact cells is less accessible due to high mass transfer resistance.

Reverchon [4] developed a model for fluid-solid extraction, where the oil is treated as a single component, and the extraction process is controlled by internal mass transfer resistance, neglecting external mass transfer. However, this model does not consider the influence of axial dispersion or changes in density and flow rate along the bed.

In this work, the fundamental governing equations are derived and combined with the kinetic model suggested by Reverchon [4] to obtain a general model for the oil extraction process from the caraway seed. This model simplifies some of the physical behaviour to obtain a control-oriented model. It is assumed that the extraction process operates semi-continuously in a cylindrical vessel. The solvent is first brought to supercritical conditions, pumped through a fixed bed of finely chopped biomass, and the solute is extracted from the biomass. The solvent and solute are then separated in a flush drum, and the extract is collected. The feed flow rate (F_{in}) and inlet temperature (T_{in}) of the extractor can be measured and manipulated, while the vessel pressure (P) can also be measured and manipulated. However, the outlet temperature (T_{out}) can only be measured. Figure 1 shows a simplified flow diagram.

This study aims to develop a process model for extracting natural substances from solid materials and liquids using supercritical fluids, specifically supercritical CO_2. To achieve this, the model parameters are estimated based on thermodynamic relations and a set of experiments conducted at various conditions. The maximum likelihood estimator

---

*Corresponding author

✉ oliwer.sliczniuk@aalto.fi (O. Sliczniuk*)

ORCID(s): 0000-0003-2593-5956 (O. Sliczniuk*); 0000-0002-0183-5558 (P. Oinas)
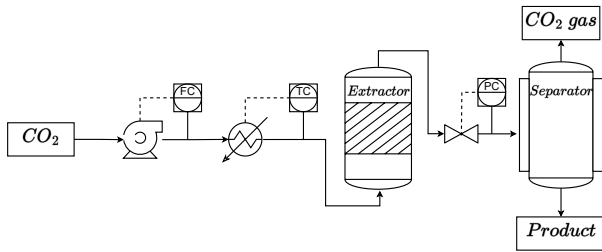
Figure 1: Process flow diagram

is used to solve the parameter estimation problem, and the obtained parameters are subjected to regression to derive correlations. These correlations enable the process model to be generalized across a range of temperatures (40 to $50°C$) and pressures (200 to 300 bars).

The study is structured as follows: Chapter 2.1 provides a general discussion on supercritical fluids to familiarize the reader with their properties. Chapter 2.2 introduces the general balance equations derived under the Low-Mach number assumption. The simplified balance equations are combined with the extraction kinetic equation to develop the process model in Chapter 2.3. The maximum likelihood technique is presented in Chapter 2.4 and is then combined with the process model. The dataset obtained from laboratory experiments closes the optimization problem in Chapter 2.5. Finally, the parameter estimations and simulation results are discussed in Chapters 3 and 4

2. Materials and methods

2.1. Supercritical fluids

A supercritical fluid (SCF) is a substance at a temperature and pressure above its critical point, where there are no distinct liquid and gas phases but below the pressure required to compress it into a solid. SCFs can move through porous solids like gases, which is faster than liquid transport through such materials. SCFs have a higher ability to dissolve materials like liquids or solids compared to gases. Near the critical point, small changes in pressure or temperature result in significant changes in density, allowing many properties of an SCF to be fine-tuned. By changing the pressure and temperature, the properties can be tuned to be more liquid-like or gas-like.

Fluid properties can be divided into two kinds: equilibrium properties and transport properties. The equation of state can be used accurately to predict the equilibrium properties, such as density, enthalpy, vapour pressure, fugacity and fugacity coefficient, vapour-liquid equilibrium, and all kinds of excess properties.

Supercritical CO_2's thermodynamic properties, such as density, the local speed of sound, and specific heat capacity, vary significantly with slight changes in temperature and pressure due to real gas effects. The Peng-Robinson equation of state (P-R EOS) is used to calculate the thermodynamic

properties by accounting for these real gas effects are presented in Appendix A.1.1. The P-R EOS belongs to a specific class of thermodynamic models for modelling the pressure of a gas as a function of temperature and density.

To determine the thermodynamic properties of a real gas, it is necessary to evaluate the departure function of the chosen equation of state for that property. As explained by Elliott [5], the departure function is the difference between the actual value of a thermodynamic property of a real gas and its value if the gas were ideal under the same temperature and pressure conditions. The ideal gas serves as a reference state to which the properties of real gases are compared. The departure function measures the extent to which a real gas deviates from ideal gas behaviour. The departure functions allow for the accurate calculation of thermodynamic properties for real gases.

The properties of CO_2 are presented as a function of operating conditions (temperature and pressure) in Figure 2. At standard atmospheric pressure and temperature, CO_2 behaves as an ideal gas, and its compressibility factor equals unity. However, at high pressures and/or low temperatures, intermolecular forces between gas molecules become more significant, causing them to deviate from ideal behaviour. As a result, the compressibility factor can be greater than or less than unity, depending on the magnitude of these forces. As presented in Figure 2a, the compressibility factor obtained from the Peng-Robinson equation of state varies strongly depending on the operating conditions.

The real gas effects are also visible on the density plot presented in Figure 2b. The density calculations are based on the compressibility factor, and its value depends on the operating conditions. The fluid properties near the critical point are unique and combine gas-like and liquid-like properties. The details of calculations are explained in the Appendix A.1.2.

Figure 2c show the behaviour of the heat capacity of a supercritical fluid at constant pressure (C_p). The details of the calculations can be found in Appendix A.1.3. Contrary to the density, which varies monotonically, the specific heat shows very high levels in a narrow region. In the subcritical region, the phase transition is associated with an effective spike in the heat capacity (i.e., the latent heat). Approaching the critical point, the latent heat falls to zero, which is accompanied by a gradual rise in heat capacity in the pure phases near phase transition. At the critical point, the latent heat is zero, but the heat capacity shows a diverging singularity. Beyond the critical point, there is no divergence, but rather a peak in the heat capacity; the highest point of this peak identifies the Widom line (as discussed by Simeoni et al. [6] and Banuti [7]).

Transport properties such as viscosity and conductivity play a crucial role in engineering design for production, fluid transportation, and processing. However, as highlighted by Sheng et al. [8], developing a satisfactory theory for transport properties of real dense gases and liquids is a challenging task. This is due to the inherent difficulties involved

(a) The compressibility factor based on the Peng-Robinson equation of state

(b) The fluid density based on the Peng-Robinson equation of state

(c) The specific heat of CO_2 based on the Peng-Robinson equation of state

(d) The enthalpy of CO_2 based on the Peng-Robinson equation of state (FONT SIZE)

(e) Thermal conductivity obtained based on Laesecke correlation

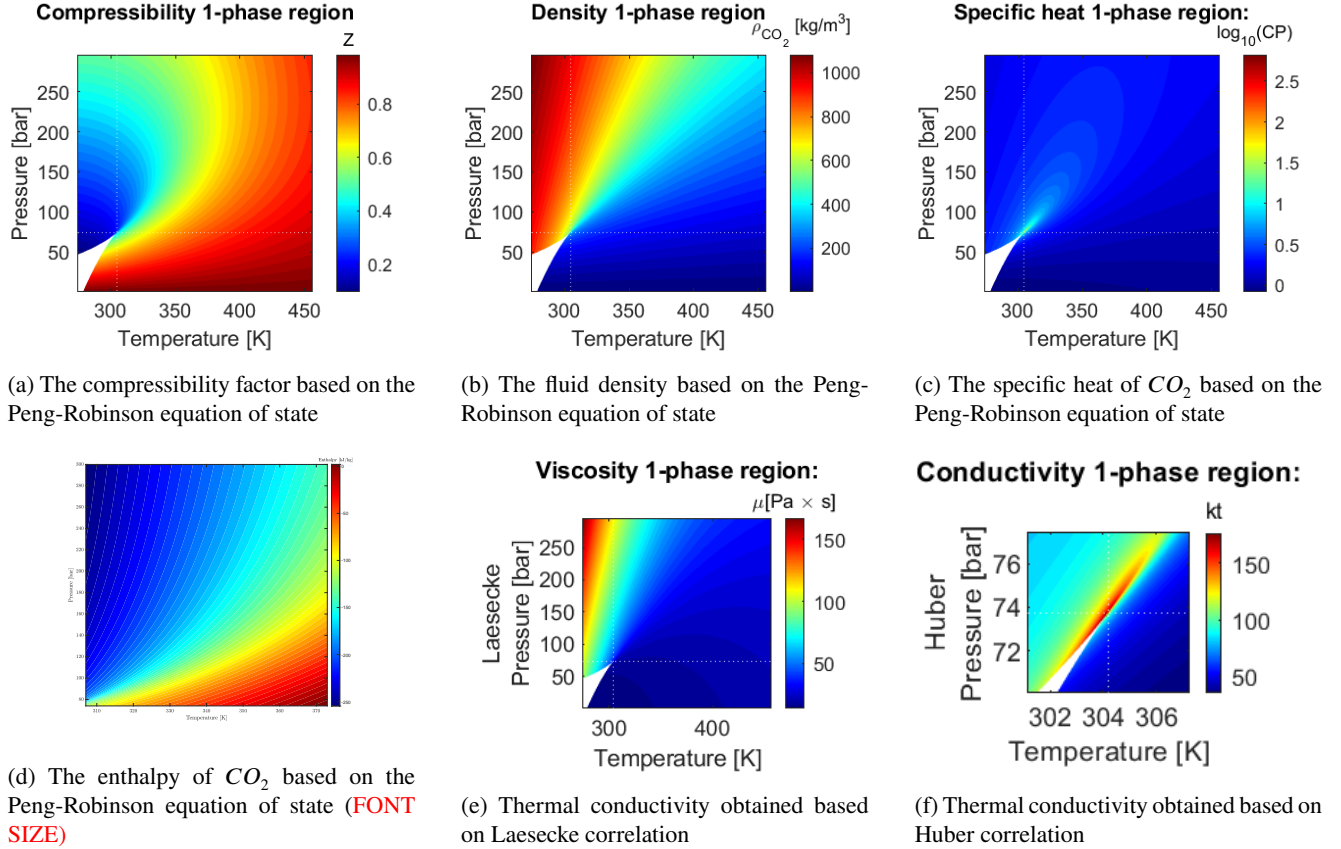(f) Thermal conductivity obtained based on Huber correlation

Figure 2: Properties of CO_2 based on the equation of state

in accurate measurements and the complexity involved in theoretical treatments.

To address this issue, the correlations of transport co-efficients are either empirical or based on some theoretical foundation. Chapman-Enskog's theory (presented in Chapman and Cowling [9]) for transport properties of dense gases based on the distribution function is a popular theoretical approach. However, the Chapman-Enskog theory was developed for rigid spherical molecules and modifications are required to apply it to real gases. Many correlations have been proposed following the Chapman-Enskog theory in the form of reduced density and reduced temperature, such as those developed by Fenghour et al. [10], and Laesecke and Muzny [11] from the National Institute of Standards and Technology (NIST). The correlation of Laesecke and Muzny [11] is presented in Figure 2e.

NIST has developed a viscosity formulation consisting of four contributions: (i) for the limit of zero density, (ii) for the initial density dependence, (iii) for the residual viscosity, and (iv) for the singularity of the viscosity at the critical point. The NIST correlation covers temperatures from 100 to 2000 K for gaseous CO_2, and from 220 to 700 K with pressures along the melting line up to 8000 MPa for compressed and supercritical liquid states. These correlations and theories are essential in predicting transport properties

for real gases and liquids and can assist in engineering design and analysis.

Similarly, the NIST developed the correlation, which describe the behaviour of thermal diffusivity of CO_2. The work of Huber et al. [12] captures the singular behaviour of thermal conductivity around the critical point. The correlation is applicable for the temperature range from the triple point to 1100 K and pressures up to 200 MPa. Figure 2f. The presented figure show regions around the critical point where the singularity is present.

2.2. Governing equations

The governing equation [1] for a quasi-one-dimensional compressible flow in Cartesian coordinates can be found in the Appendix A.2 and in the work of Anderson [13]. Quasi-one-dimensional flow is a fluid flow characterized by the assumption that the flow properties remain uniform across any given cross-section of the flow. This assumption is made when there is a variation in the cross-sectional area of the flow channel, such as an irregular shape or partial filling of an extractor. In such cases, the flow is considered to be quasi-one-dimensional because the velocity and other flow properties are assumed to vary only in the direction of flow.

---

[1]For the sake of clarity of the process model, different colors have been used in the equations to indicate: control variables, state variables, variables and parameters.

The quasi-one-dimensional compressible Navier-Stokes equations in Cartesian coordinates are given by Equations 1 to 3. The derivation of these Equations are presented in Appendix A.2.

$$\frac{\partial\left(\rho_f A_f(z)\right)}{\partial t} + \frac{\partial\left(\rho_f A_f(z)v\right)}{\partial z} = 0 \tag{1}$$

$$\frac{\partial\left(\rho_f v A_f(z)\right)}{\partial t} + \frac{\partial\left(\rho_f A_f(z)v^2\right)}{\partial z} = -A_f(z)\frac{\partial P}{\partial z} \tag{2}$$

$$\frac{\partial\left(\rho_f e A_f(z)\right)}{\partial t} + \frac{\partial\left(\rho_f A_f(z)ve\right)}{\partial z} = -P\frac{\left(A_f(z)v\right)}{\partial z} + \frac{\partial}{\partial z}\left(\frac{\partial T}{\partial z}\right) \tag{3}$$

where ρ_f is the density of the fluid, $A_f(z)$ is the function which describe change of the cross-section, v is the velocity, P is the total pressure, e is the internal energy of the fluid, t is time and z is the spacial direction.

Based on governing equations, the small discontinuity (defined as δ) in flow properties, shown in Figure 3, can be analysed. The analysis follows the work of Schreier [14].

	ρ_f	$\rho_f + \delta\rho_f$	
$v \rightarrow$	P	$P + \delta P$	$v + \delta v \rightarrow$
	T	$T + \delta T$	

Figure 3: Small discontinuity in one-dimensional flow

The discontinuity is presumed to be at rest relative, and the balance equations become

$$\rho_f \delta v + v\delta\rho_f + \delta\rho_f\delta v = 0$$

$$\delta P = \delta v\delta\rho_f$$

These relations are equally valid if the two regions are separated by a region of finite width rather than a discontinuity.

$$\lim_{\rho_f v \to 0} \rho_f\delta v + v\delta\rho_f + \delta\rho_f\delta v = 0/\delta\rho_f \rightarrow \frac{dv}{d\rho_f} = -\frac{v}{\rho_f}$$

By combining the momentum equation with the above equation, we get

$$\frac{dv}{d\rho_f} = -\frac{dv}{dP}\frac{dP}{d\rho_f} = -\frac{1}{\rho v}\frac{dP}{d\rho_f} = -\frac{v}{\rho_f} \tag{4}$$

Suppose the flow is presumed to be isentropic, $dP/d\rho_f = c^2$, so $v^2 = c^2$, where c is the speed of sound. This can be interpreted as a small pressure wave propagating with the speed of sound relative to the flow. Moreover, if the flow velocity is relatively low, all pressure changes are hydrodynamic (due to velocity motion) rather than thermodynamic which leads to $\partial\rho_f/\partial P \approx 0$. In other words, the small changes in pressure due to flow velocity changes do not change the density. This has a secondary effect – the speed of sound in the fluid is $\partial P/\partial\rho_f = \infty$ in this instance. So there is an infinite speed of sound, which makes the equations elliptic in nature. It can be deduced that at the isothermal conditions, the density in the system propagates with the same speed as pressure since they are both connected through the equation of state. The details of the Mach-number analysis are presented in Appendix A.3.

2.3. Extraction model
2.3.1. Continuity equation

The obtained above quasi-one-dimensional continuity equation (Equation 1) is further modified by specifying a function $A_f(z) = A_f\phi(z)$ to take into account the change of the cross-section available for the fluid. The cross-section change is taken into account by void fraction $\phi(z)$, which depends on the spatial dimension. The equation 5 shows the differential form, of the continuity equation:

$$\frac{\partial(\rho_f(T(t,z),P(t))\phi(z))}{\partial t} + \frac{\partial(\rho_f(T(t,z),P(t))vA\phi(z))}{\partial z} = 0 \tag{5}$$

where A is the total cross-section of the extractor.

assign a color of v and u

Assuming that the mass flow rate is constant in time, the temporal derivative becomes zero, and the spatial derivative can be integrated along z as

$$\int\frac{\partial(\rho_f(T(t,z),P(t))vA\phi(z))}{\partial z}dz = 0 \rightarrow F = \rho_f(T(t,z),P(t))vA\phi(z) \tag{6}$$

Here, F is a constant obtained from the integration and is understood as the mass flux per unit area, which is assumed to be constant along z. To simplify the dynamics of the system, it is assumed that $F = F(t)$ is a control variable and affects the whole system instantaneously. This assumption allows for finding the velocity profile that satisfies mass continuity based on $F(t)$, $\phi(z)$, and $\rho_f(T(t,z),P(t))$.

$$v = \frac{F(t)}{\rho_f(T(t,z),P(t))A\phi(z)} \tag{7}$$

The fluid density $\rho_f(T(t,z),P(t))$ can be obtained from an equation of state if temperature and the thermodynamic pressure (assumed $P(t)$ to be constant along z due to the low-Mach number condition) are known. The variation in density may be caused by the fluid accumulation in the system (equivalent to pressure change), which occurs instantaneously along z or by a temperature change.

Analogously, the superficial velocity might be introduced to the model and defined as

$$u = v\phi(z) = \frac{F(t)}{\rho_f(T(t,z),P(t))A} \tag{8}$$

2.3.2. Mass balance for the fluid phase

The detailed derivation of the mass balance equation for the fluid phase can be found in the appendix (A.2). The movement of the mobile pseudo-homogeneous phase (Equation 9) is considered only in the axial direction, while the properties of the system in the radial direction are assumed to be uniform. Additionally, the boundary layer adjacent to the inner wall of the extractor is neglected, resulting in a constant velocity profile across any cross-section of the extractor perpendicular to the axial direction. Although the particle size distribution and void fraction of the solid phase may change along the extractor, they are assumed to remain constant in time. Furthermore, the thermodynamic pressure is assumed to be constant along the device due to the Low-Mach number condition, as previously discussed.

The amount of solute in the solvent is considered negligible, resulting in the fluid phase being described as pseudo-homogeneous, and its properties are assumed to be the same as the solvent. The mass balance equation for the fluid phase includes convection, diffusion, and kinetic terms.

$$\frac{\partial c_f(t,z)}{\partial t} + \frac{1}{\phi(z)}\frac{\partial\left(c_f(t,z)u\right)}{\partial z} = \frac{1-\phi(z)}{\phi(z)}r_e(t,z) + \frac{1}{\phi(z)}\frac{\partial}{\partial z}\left(D_e^M\frac{\partial c_f(t,z)}{\partial z}\right)$$

(9)

Here, $c_f(t,z)$, $c_s(t,z)$, and $T(t,z)$ represent the concentration of solute in the fluid phase, the concentration of solute in the solid phase, and temperature, respectively. $r_e(t,z)$ is a mass transfer kinetic term, $F(t)$ is the mass flow rate and $D_e^M(T(t,z),P(t),F(t))$ is the axial mass diffusion coefficient.

2.3.3. Mass balance for the solid phase

The solid phase is considered to be stationary, with negligible convection and diffusion terms in the mass balance equation (Equation 10). Therefore, the only significant term in this equation is the kinetic term (as defined in Equation 11), which connects the solid and fluid phases. The extract is represented by a single pseudo-component to simplify the analysis.

$$\frac{\partial c_s(t,z)}{\partial t} = \underbrace{r_e(t,z)}_{\text{Kinetics}}$$

(10)

2.3.4. Kinetic term

The kinetic term in this study is based on the two-film theory proposed by Reverchon [4], and the mass transfer kinetic is given by Equation 11. This equation takes into account the overall diffusion coefficient and the concentration gradient, which acts as the driving force for the process.

As the solvent flows through the bed, CO_2 molecules diffuse into the pores and adsorb on the particle surface to form an external fluid film around the solid particles due to the solvent-solid matrix interactions. The effect of Knudsen diffusion is negligible in this process, as the mean free path of the molecule is much smaller than the pore diameter. The dissolved solute diffuses from the particle's core through the solid-fluid interface, the pore, and the film into the bulk. Figure 4 illustrates the mass transfer mechanism, where the mean solute concentration in the solid phase is denoted as c_s and the equilibrium concentrations at the solid-fluid interface are denoted as c_s^* and c_P^*, respectively, for solid and fluid phases. The concentration of the solutes in the fluid phase in the center of the pore is denoted as c_P. As the solute diffuses through the pore, its concentration changes and reaches c_{Pf} at the opening of the pore. The solute then diffuses through the film around the particle and reaches a concentration in bulk c_f. The two-film theory describes the solid-fluid interface inside the pore. The overall mass transfer coefficient can be determined if the relationship between the solute concentration in one phase and its equilibrium concentration is known.

Bulley et al. [15] suggests a process where the driving force for extraction is given by the difference between the
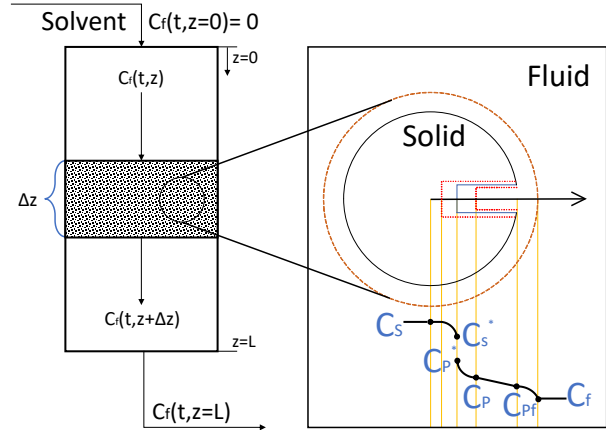

Figure 4: The extraction mechanism

concentration of the solute in bulk, c_f, and in the center of the pore, c_P^*. The concentration c_P^* is in equilibrium with c_s according to an equilibrium relationship. The rate of extraction is thus $r_e\left(c_f - c_P^*(c_s)\right)$.

On the other hand, Reverchon [4] proposes a driving force given by the difference between c_s and c_P^*. c_P^* is determined by an equilibrium relationship with c_f and the extraction rate is $r_e\left(c_s - c_P^*(c_f)\right)$ or more precisely

$$r_e(t,z) = \frac{D_i(T(t,z),P(t))}{\mu l^2}\left(c_s(t,z) - c_P^*(t,z)\right)$$

(11)

where μ is sphericity, l a characteristic dimension of particles and can be defined as $l = r/3$, r is the mean particle radius, ρ_s is the solid density, $D_i(T(t,z))$ corresponds to the overall diffusion coefficient and $c_P^*(t,z)$ is a concentration at the solid-fluid interface (which according to the internal resistance model is supposed to be at equilibrium with the fluid phase).

According to Bulley et al. [15], a linear equilibrium relationship (equation 12) can be used to find an equilibrium concentration of the solute in the fluid phase $c_f^*(t,z)$ is based on the concentration of the solute in the solid phase $c_s(t,z)$

$$c(t,z) = k_p(T(t,z),P(t))q^*(t,z)$$

(12)

The volumetric partition coefficient $k_p(T(t,z),P(t))$ behaves as an equilibrium constant between the solute concentration in one phase and the corresponding equilibrium concentration at the solid-fluid interphase. According to Spiro and Kandiah [16], the term $k_p(T(t,z),P(t))$ can be expressed as the function of mass partition factor $k_m(T(t,z))$.

$$k_m(T(t,z)) = \frac{k_p(T(t,z),P(t))\rho_s}{\rho(T(t,z),P(t))}$$

(13)

Equation 14 represents of the kinetic term according to Reverchon [4]

$$r_e(t,z) = -\frac{D_i(T(t,z),P(t))}{\mu l^2}\left(c_s(t,z) - \frac{\rho_s}{k_m(T(t,z))\rho_f(T(t,z),P(t))}c_f(t,z)\right)$$

(14)

2.3.5. Uneven distribution of the solute in the solid phase

Following the idea of the Broken-and-Intact Cell (BIC) model presented by Sovova [21], the coefficient γ is introduced to limit the available oil. The $\gamma(c_s(t, z))$ describes the decay function, which is equal to unity and slowly decays when the amount of the solute in the solid phase decrease. Similarly to the BIC model, this can be explained if oil is assumed to be contained in the cells, a part of which is open because the cell walls were broken by grinding, and the rest remains intact. The γ parameter multiply the internal diffusion term to indicate that the diffusion of the solute from a particle's core takes more time compared to the diffusion of the solute located close to the outer surface.

$$\gamma(c_s(t, z)) = \exp\left(\Upsilon\left(1 - \frac{c_s(t, z)}{c_{s0}}\right)\right) \tag{15}$$

where the Υ describe the curvature of the decay function. The final form of the extraction kinetic equation is given by equation 16.

$$r_e(t, z) = -\frac{D_i(T(t, z), P(t))\gamma(c_s(t, z))}{\mu l^2}\left(c_s(t, z) - \frac{\rho_s}{k_m(T(t, z))\rho(T(t, z), P(t))}c_f(t, z)\right) \tag{16}$$

2.3.6. Heat balance

The heat equation was introduced in the previous chapter through Equation 3, in the appendix A.2 as well as through Equation 17

$$\frac{\partial\left(\rho_f(T(t, z), P(t))e(t, z)A_f\right)}{\partial t} + \frac{\partial\left(\rho_f(T(t, z), P(t))A_f v e(t, z)\right)}{\partial z}$$
$$= -P(t)\frac{(A_f v)}{\partial z} + \frac{\partial}{\partial z}\left(\frac{\partial T(t, z)}{\partial z}\right) \tag{17}$$

Following Elliott [5] or Gmehling et al. [17], a real gas internal energy definition can be obtained from the departure functions, defined through Equation 18. In thermodynamics, the departure function is a mathematical function that characterizes the deviation of a thermodynamic property of a real substance from that of an ideal gas at the same temperature and pressure. The departure function is typically defined as the difference between the value of a thermodynamic property for a real fluid and the corresponding value for an ideal gas at the same temperature and pressure. Common departure functions include those for enthalpy, entropy, and internal energy. They are typically computed by integrating a function that depends on the equation of state and its derivatives. More information on the departure functions can be found in appendix A.1.4.

$$de(t, z) = C_v dT - \left[P(t) - T(t, z)\left(\frac{\partial P(t)}{\partial T(t, z)}\right)_{v_m(T(t, z), P(t))}\right]dv_m(T(t, z), P(t)) \tag{18}$$

where $e^{id}(t, z)$ is the internal energy of perfect gas.

Suppose a gas is considered to be perfectly caloric ($e(t, z) = C_v T(t, z)$), then the energy equation can be written explicitly in the form of temperature. The perfectly caloric gas can be seen as the special case of a real gas, where

the second term of Equation 18 goes to zero and the heat capacity C_v is constant.

For real gases, it is complicated to write the heat balance in terms of temperature, but it be can be used directly in the form of internal energy, as it is given by Equation 3. In such a case, the temperature needs to be recovered from the internal energy. A relation for the internal energy can be obtained from an equation of state. For Peng-Robinson, such a relation is given by Equation 19 as presented by Elliott [5].

$$\frac{e(t, z) - e^{id}(t, z)}{RT(t, z)} =$$
$$-\frac{A(T(t, z), P(t))}{B(T(t, z), P(t))\sqrt{8}}\frac{\kappa\sqrt{T_r}}{\sqrt{\alpha}}\ln\left[\frac{Z(T(t, z), P(t)) + \left(1 + \sqrt{2}\right)B(T(t, z), P(t))}{Z(T(t, z), P(t)) + \left(1 - \sqrt{2}\right)B(T(t, z), P(t))}\right] \tag{19}$$

To solve Equation 19, temperature, pressure, and density values need to be known. If an equation of state is introduced, then only two out of three variables need to be obtained as the third one can be calculated; this can be represented as follow

$$e(t, z) = e(T(t, z), P(t), \rho_f(T(t, z), P(t))) = e(T(t, z), P(t), \rho_f(T(t, z), P(t))) \tag{20}$$

If the value of internal energy $e(t, z)$ is known from the time evolution of the energy Equation 3, and pressure is known from measurement, then the temperature can be reconstructed. A roootfinder can be used to find a value of temperature, which minimizes the difference between the value of internal energy coming from the time evolution (Equation 17) and the output from Equation 19. Such a procedure allow to find local temperature along spatial direction z and needs to be repeated every time-step.

Another way to express the energy equation is to introduce enthalpy $h(t, z) = e(t, z) + P(t)/\rho_f(T(t, z), P(t))$. By introducing the definition of enthalpy, the energy equation becomes

$$\frac{\partial\left(\rho_f(T(t, z), P(t))h(t, z)A_f\right)}{\partial t} - \frac{\partial\left(P(t)A_f\right)}{\partial t}$$
$$+ \frac{\partial\left(\rho_f(T(t, z), P(t))h(t, z)A_f v\right)}{\partial z} - \frac{\partial}{\partial z}\left(k\frac{\partial T(t, z)}{\partial z}\right) \tag{21}$$

The main advantage of this formulation is the presence of term $\partial P(t)/\partial t$, which allows it to directly affect the system through the change of thermodynamic pressure (which is a control variable). If an equation of state is known, the temperature can to be recovered from the enthalpy. The enthalpy is related to the pressure and temperature through the following equation:

$$h(t, z) = h(T(t, z), P(t), \rho_f(T(t, z), P(t))) = h(T(t, z), P(t), \rho_f(T(t, z), P(t))) \tag{22}$$

If the value of enthalpy is known from the time evolution and pressure can be measured, then the Equation 22 can be solved for the temperature to recover the temperature profile. By applying the departure functions to Peng-Robinson equation of state, the relation 22 can be expressed

directly through Equation 23 as presented in A.1.4 or given by Gmehling et al. [17].

$$h(t,z) - h(t,z)^{id} = RT(t,z)\left[T_r(Z(T(t,z),P(t)) - 1)\right]$$

$$-2.078(1+\kappa)\sqrt{\alpha(T(t,z))}\ln\left(\frac{Z(T(t,z),P(t)) + \left(1+\sqrt{2}\right)B(T(t,z),P(t))}{Z(T(t,z),P(t)) + \left(1-\sqrt{2}\right)B(T(t,z),P(t))}\right) \quad (23)$$

The Equation 23 requires an reference sate, which in this case is assumed to be $T_{ref} = 298.15\ [K]$ and $P_{ref} = 1.01325\ [bar]$.

As discussed by Gmehling et al. [17], special attention should be paid to high pressures systems, so the influence of the intermolecular forces on the enthalpy is taken into account. In most cases, these forces are attractive, so additional energy is necessary to move the molecules away from each other, that is, to lower the density. If this energy is not added, the substance cools down when it is expanded.

2.3.7. Pressure term

The pressure term in the energy equation, given by Equation 21, describes the change of the thermodynamic pressure with respect to time. As explained in Chapters A.2 and A.3, at low-Mach number conditions, the thermodynamic pressure is nearly constant in space due to the small pressure wave propagation that occurs at the speed of sound. Under such conditions, the term $\partial P/\partial t$ can be approximated by an ordinary differential equation, which describes the instantaneous change of pressure in the system. The pressure in the system is considered a state variable, while the pressure in the new time-step is considered a control variable.

$$\frac{\partial P(t)}{\partial t} \approx \frac{P(t) - P_{in}(t)}{\Delta t} \quad (24)$$

Such a simplified equation takes into account the pressure change in the energy balance, but the dynamics are simplified and do not consider the effects of pressure losses. In a real system, the pressure change dynamics would depend on the pump used in the system, as well as the back-pressure regulator used to control the outlet valve.

2.3.8. Extraction yield

The efficiency of the process (the yield) is calculated according to equations 25 as presented by Sovova et al. [18]. The measurement equation evaluate the mass of solute at the outlet of the extraction unit and sums it. The integral form of the measurement equation (25) can be transformed into the differential form (26) and augmented with the process model.

$$y(t) = \int_{t_0}^{t_f} \frac{F(t)}{\rho_f(T(t,z),P(t))} c_f(t,z)\Big|_{z=L} dt \quad (25)$$

$$\frac{dy(t)}{dt} = \frac{F(t)}{\rho_f(T(t,z),P(t))} c_f(t,z)\Big|_{z=L} \quad (26)$$

2.3.9. Initial and boundary conditions

It is assumed that the solvent is free of solute at the entrance of the extractor and that all the solid particles have the same initial solute content c_{s0}. The fluid concentration

is assumed to not be uniform, and as such it is described by a function $H = H(z)$. The further discussion on the distribution of concentration in the fluid phase can be found in appendix A.6. Moreover, it is considered that the initial temperature of the extractor in every place is the same and described by h_0. Therefore, the initial conditions employed in the simulation are:

$$c_f(t=0,z) = H(z)$$
$$c_s(t=0,z) = c_{s0}$$
$$h(t=0,z) = h_0$$

2.3.10. State-space representation

The process model can be written in a general form:

$$\begin{bmatrix} \dfrac{\partial c_f(t,z)}{\partial t} \\ \dfrac{\partial c_s(t,z)}{\partial t} \\ \dfrac{\partial h(t,z)}{\partial t} \\ \dfrac{\partial y(t)}{\partial t} \end{bmatrix} = \begin{bmatrix} \bar{\phi}_1\left(c_f(t,z),c_s(t,z),h(t,z);\Theta\right) \\ \bar{\phi}_2\left(c_f(t,z),c_s(t,z),h(t,z);\Theta\right) \\ \bar{\phi}_3\left(c_f(t,z),c_s(t,z),h(t,z);\Theta\right) \\ \bar{\phi}_4\left(c_f(t,z),c_s(t,z),h(t,z);\Theta\right) \end{bmatrix} = \bar{\phi}(t,z;\Theta) = \frac{\partial \chi(t,z)}{\partial t}$$

$$(28)$$

where Θ is a paramter space consisting of model parameters θ and controls u, $\bar{\phi}$ is a set of functions that correspond to state equations of the model, and χ is the state-space model.

Each function $\bar{\phi}_i$ is transformed to a corresponding set of N_z discretized equations denoted as $G_{i \times N_z + 1}$ to $G_{(i+1) \times N_z}$, where i corresponds to the process model equation. The state-space model $\chi(t,z)$ after the discretization is represented by $\dot{x}(t)$.

$$\dot{x}(t) = \frac{dx(t)}{dt} = \begin{bmatrix} \dfrac{dc_{f,1}(t)}{dt} \\ \vdots \\ \dfrac{dc_{f,N_z}(t)}{dt} \\ \hline \dfrac{dc_{s,1}(t)}{dt} \\ \vdots \\ \dfrac{dc_{s,N_z}(t)}{dt} \\ \hline \dfrac{dh_1(t)}{dt} \\ \vdots \\ \dfrac{dh_{N_z}(t)}{dt} \\ \hline \dfrac{dy(t)}{dt} \end{bmatrix} = \underbrace{\begin{bmatrix} G_1\left(c_f(t),c_s(t),h(t);\Theta\right) \\ \vdots \\ G_{N_z}\left(c_f(t),c_s(t),h(t);\Theta\right) \\ \hline G_{N_z+1}\left(c_f(t),c_s(t),h(t);\Theta\right) \\ \vdots \\ G_{2N_z}\left(c(t),c_s(t),h(t);\Theta\right) \\ \hline G_{2N_z+1}\left(c_f(t),c_s(t),h(t);\Theta\right) \\ \vdots \\ G_{3N_z}\left(c_f(t),c_s(t),h(t);\Theta\right) \\ \hline G_{3N_z+1}\left(c_f(t),c_s(t),h(t);\Theta\right) \end{bmatrix}}_{G(x(t);\Theta)}$$

where $x \in \mathbb{R}^{N_x = 3N_z}$ and $\Theta \in \mathbb{R}^{N_\Theta = N_\theta + N_u}$, N_θ is the number of model parameters, N_u is the number of control variables.

In a state-space sense, the state variables of the system are the local concentrations of solute in the fluid and solid phases ($c_f(t,z)$ and $c_s(t,z)$, respectively), and the

local enthalpy of the pseudo-homogeneous phase ($h(t, z)$). The controllable input variables are the mass flow-rate and temperature of the solvent in the feed and the pressure in the extractor. We extend the system state-space by assuming that extraction yield can be modelled as a function of a known initial mass of solute in the solid phase and it can be measured after the separator ($Y(t)$). The system is controllable by manipulating the flow-rate and temperature (enthalpy) of CO_2 in the feed, and the pressure in the extractor.

2.3.11. Discretization methods

The method of lines is used to transform the process model equations into a set of ODEs denoted as $G(x(t); \Theta)$. The partial derivatives in z-direction are computed using a first-order and second-order finite difference approximation. The backward finite difference is used to approximate the first-order derivative, while the central difference scheme is used to approximate the second-order derivative. The length of the fixed bed is divided into N_z equally distributed points in z-direction.

As presented in Appendix A.2, all the governing can be written in the integral form using the Divergence Theorem. The integral equation states that the change rate of the integral of any quantity over an arbitrary control volume is given by the flux through the boundary of the control volume, with being the outer surface normal through the boundary. That quantity is neither produced nor consumed inside of the control volume and is hence conserved. For a derivative to be conservative, it must form a telescoping series. In other words, after the addition of all terms coming from the discretization over a grid, only the boundary terms should remain and the artificial interior points should cancel out. To ensure the mass conservation, the discretization is applied on the conservative form of the process model.

2.4. Parameter estimation

The goal of parameter estimation is to obtain the "best" estimate of parameter set θ (which is a subset of the parameter space Θ containing all parameters of a model) based on the continuous observations $Y(t)$ or the discrete observations $Y(t_i)$. Conceptually, the unobservable error $\epsilon(t)$ is added to the deterministic model output, $y(t)$ (Equation 25), to give the observable dependent variable $Y(t)$ (for example results of an experiment). For discrete observations, this can be expressed as:

$$Y(t_i) = y(\theta, t_i) + \epsilon(t_i)$$

For continuous variables, the equation is:

$$Y(t) = y(\theta, t) + \epsilon(t)$$

However, obtaining analytical solutions for a deterministic process model can be challenging, so experiments are often conducted where the vector of derivatives $dY(t_i)/dt$ is measured instead of $Y(t_i)$ itself. In such cases, it is assumed that the unobservable error is added to the deterministic derivative $dy(\theta, t_i)/dt$ as shown below

$$\frac{dY(t_i)}{dt} = \frac{dy(\theta, t_i)}{dt} + \epsilon(t_i) \tag{29}$$

In the case where the error in the first observation is denoted as ϵ_1, the error in the second observation ϵ_2' incorporates ϵ_1 as well as an independent random component, given by $\epsilon_2' = \epsilon_1 + \epsilon_2$. Similarly, the error in the third observation is $\epsilon_3' = \epsilon_1 + \epsilon_2 + \epsilon_3$, and so on. Mandel [19] made a distinction between the typically assumed independent measurement error in the dependent variable and a "cumulative" or interval error, in which each new observation encompasses the error of the previous ones. Cumulative errors arise from fluctuations in the process itself due to small variations in operating conditions and are not independent; only the differences in measurement from one period to the next are independent.

Maximum likelihood estimation (MLE) is a statistical method used to estimate the parameters of a probability distribution based on observed data. The MLE works by finding the values of the parameters that maximize the likelihood function, which is the probability of observing the given data for a given set of parameter values. The MLE has desirable properties such as asymptotic efficiency and normality. Although the MLE has often been associated with the normal distribution for mathematical convenience, it can be applied to a wide range of probability distributions. The derivation of the likelihood function under the assumption of the Gaussian distribution is presented in Appendix A.7. The final form of the objective function is presented by Equation 30:

$$\ln L = -\frac{n}{2}\left(\ln\sqrt{2\pi} + \ln\sigma^2\right) - \frac{\sum_{i=1}^{n}\left[\frac{dY(t_i)}{dt} - \frac{dy(\theta, t_i)}{dt}\right]^2}{2\sigma^2} \tag{30}$$

The parameter estimation problem can be formulated as follow:

$$
\begin{aligned}
\hat{\theta}_{MLE} &= \arg\max_{\sigma,\theta\in\Theta} \ln L = \arg\max_{\sigma,\theta\in\Theta} p(\theta|y) \\
\text{subject to} \quad & \dot{x} = G(x(t); \theta) \\
& \dot{\theta} = 0 \\
& y = y(t) \\
& \theta^{lb} \leq \theta \leq \theta^{ub}
\end{aligned}
\tag{31}
$$

where $\hat{\theta}$ is as maximum likelihood estimator, θ^{lb} define the minimal value of θ and θ^{ub} is the maximum value of θ.

Based on the first order optimality condition, the $\ln L$ can be maximized with respect to the vector θ and equating to zero the partial derivatives of $\ln L$:

$$\frac{\partial \ln L}{\partial \theta} = \frac{\partial \sum_{i=1}^{n} \ln p\left(y(t_i)|\theta\right)}{\partial \theta} = 0 \tag{32}$$

Solution of Equations 32 yield the desired estimates $\hat{\theta}$. For some models, these equations can be explicitly solved for $\hat{\theta}$ but in general, no closed-form solution to the maximization problem is known or available, and a maximum likelihood estimator can only be found via numerical optimization.

2.5. Experimental work

In order to solve the optimization problem presented in Equation 31, it is necessary to have knowledge of the dataset $Y(t)$, which was obtained by extracting caraway oil from caraway seeds. To prepare the seeds for extraction, they were first pre-treated using a Retsch SM 300 cutting mill to

reduce their particle size to 1mm and break their outer shell. The moisture content of the seeds was then determined using an Infrared Moisture Analyser, which revealed an average moisture content of 4.83% in the solid particles after grinding. Next, the density of the solid material was measured using a pycnometer, which can be found in appendix A.8. Finally, the material's porosity was also calculated to be 0.5, as explained in appendix A.9.

The caraway seeds used in the experiments were obtained from Caraway Finland during the 2022 harvesting season. The experiments were conducted using a 10-litre extractor with an inner diameter of approximately 15 cm and a height of 60 cm, which was rented from VTT Bioruukki. Four experiments were performed under different operating conditions: $40°C/200$ bar, $50°C/200$ bar, $40°C/300$ bar, and $50°C/300$ bar. The volumetric flow rate used in all experiments was on average 0.4 litres per minute, with negligible variations (up to 5%). The amount of solid material used for extraction was 1 kg (or 1.6 litres), which was not enough to fill the entire extraction chamber.

After loading the material into the extraction chamber, the extractor was pre-heated to the desired temperature. The outlet line was then closed, and the extraction chamber was filled with CO_2. The CO_2 was pumped and compressed until the desired operating pressure was reached. When the operating temperature and pressure were achieved, the outlet line was opened, allowing the solvent to flow through the system. The solvent extracted the essential oils from the solid material, and the resulting CO_2 and oil mixture flowed from the extractor to the separator. The separator operated at $50°C$ and 50 bar. The gaseous CO_2 exited from the top and was recycled to the CO_2 storage tank. The oil stayed at the bottom of the separator in the liquid form. The extraction time for each batch was 150 minutes, measured from the opening of the extractor outlet port. Every 5 minutes, the oil was drained from the separator, and its weight was measured. The resulting time series $Y(t)$ corresponds to the output of measurement Equation 25 and can be used for parameter estimation.

The results of experiments are presented in the Table 1.

3. Results

The parameter estimation problem was solved by fitting the process model to the dataset given in the Table 1. Each time-series was fitted to the model separately. As a result of fitting, the following parameters were obtained:

- Partition coefficient: k_m
- Internal diffusion coefficient: D_i
- Axial diffusion coefficient: D_e^M
- Decay curvature coefficient: Υ
- Standard deviation: σ

Time [min]	40[C]200[bar]	50[C]200[bar]	40[C]300[bar]	50[C]300[bar]
0	0	0	0	0
5	1.7	1.8	1.1	1.2
10	5.7	4.7	4.7	4.5
15	10.9	9.5	10.8	11.3
20	17.8	15.1	20.6	20.6
25	24.9	21.3	32.1	30.6
30	30.3	26.9	40.5	37.8
35	34	30.1	46.7	43.3
40	37.5	33.1	50.5	47.5
45	40.1	35.8	53.1	50.8
50	42.8	38.7	55.5	53.7
55	45.2	41.3	57.6	56.5
60	47.6	43.8	59.3	58.1
65	49.6	46.1	60.9	59.6
70	51.2	48.2	62.2	61.1
75	52.9	50.2	63.7	62.7
80	54.4	52.4	64.9	64.4
85	55.8	54.3	66.6	65.8
90	56.7	56.3	67.6	66.7
95	57.7	58	68.9	67.4
100	58.6	59.3	69.7	68.2
105	59.6	60.3	70.6	69.1
110	60.4	61.4	71.2	70.1
115	61.4	62.5	71.9	70.9
120	62.4	63.4	72.3	71.6
125	63.3	64.2	72.8	72.3
130	64	64.7	73.2	72.9
135	64.8	65.3	73.6	73.5
140	65.7	66	74	74
145	66.2	66.6	74.3	74.5
150	66.8	67.2	74.6	74.9

Table 1
Yield data; cumulative amount of solute [g] collected every 5 min

Moreover, the initial state estimation was performed together with parameter estimation. The initial solute concentration in the solid phase is assumed to be uniformly distributed. On the other hand, the solute concentration in the fluid phase should not follow the same assumption as the solid phase. During the preparation period, the solute diffuses to the fluid phase in contact with the solid particles. Later, the solute in the fluid phase is partially moved along the extractor (if the pressure increase in the system, the pump cause the movement of the fluid, even if the outlet valve is closed). As a result, the distribution of solute mass in the fluid phase is assumed not to be uniform. Some conclusions can be drawn from the analysis of the initial part of each yield curve obtained from the laboratory. It can be noticed that each curve at the beginning has a curvature, which is not linear. Generally, a quadratic function could approximate the initial part of each extraction curve. A function that, after integration, gives a quadratic-like result is a straight line. Based on that observation, the solute concentration in the fluid phase is assumed to be linearly distributed. The solute concentration is assumed to be zero at the outlet and reach the maximum at the beginning of the fixed bed. The details on the calculation are given in appendix A.6. The linear distribution can be defined if the total mass of solute m_{total} and partition coefficient τ are known.

Due to initial state estimation, two additional parameters are fitted.

- Total mass of solute: m_{total}
- Partition coefficient: τ

Parameter	k_m[-]	D_i[m/s²]	D_e^M[m/s²]	Υ [m³/kg]	m_{total}[g]	τ[-]	σ[-]
Lower bound	0	0	0	0	80	0	0
Upper bound	$+\infty$	$+\infty$	$+\infty$	100	150	1	$+\infty$
Initial guess	1e5	3	1	0	80	0.65	0.1

Table 2
Constraints and initial guess of the parameter estimation problem

Parameter	40[C]200[bar]	50[C]200[bar]	40[C]300[bar]	50[C]300[bar]
k_m[−]	74548.03812	180215.6677	99579.96492	100000.0373
D_i[m²/s] × 1e − 14	4.313	3.33282	14.3713	9.94303
D_e^M[m²/s] × 1e − 6	7.5521	7.73584	3.88465	5.72401
Υ	1.07602	0.29235	2.11194	1.51152
τ[−]	0.72426	0.76251	0.71084	0.68873
σ[−]	0.06968	0.12273	0.06887	0.05336

Table 3
Parameter estimation results rounded to fifth decimal place

To ensure that parameters found by the optimizer do not reach unrealistic values, an additional set of inequality constraints is introduced. The lower and upper bounds for each parameter are given in Table 2. To ensure that the solution is a global solution multiple initial points have been tested but presented results come from the initial guess given also in Table 2.

Figure 5 show yield curves for each of experiments. The blue dots indicate the data point obtained as a measurement from the laboratory experiments. The black curve represents the yield curve obtained from the initial guess of the parameters. The blue curve correspond to yield curve obtained as a solution of the optimization problem. The curves on the left hand-side of the Figure 5, are the cumulative yield curves, which represents the cumulative amount of the oil collected during each experiment. The plots on the right hand-side, represent the derivative of the cumulative yield curves. As explained in the chapter 2.4, the derivatives of the cumulative measurements are independent on the previous measurement and should be used for the parameter estimation.

The results of parameter estimation can be found in Table 3 and the concentration profiles, which correspond for the optimized solution for each experiments, are presented on Figure 12 in Appendix A.10. As can be noticed, the optimizer found that the partition factor should be as high as possible. Such a behaviour suggest that the solvent is far from the saturation, and the model can be simplified. The model reduction can be introduced by considering the limit of the concentration gradient

$$\lim_{k_m \to \infty} \left(c_s(t,z) - \frac{\rho_s}{k_m(T(t,z))\rho(T(t,z),P(t))} c_f(t,z) \right) =$$
$$= \left(c_s(t,z) - \frac{\rho_s}{\infty\rho(T(t,z),P(t))} c_f(t,z) \right) = \left(c_s(t,z) - 0 \right)$$

Values of the internal diffusion coefficients are distinguished for each experiment, which grows as the fluid density increase. The order of magnitude of D_i obtained from the optimization is similar to values found by other researchers. Reverchon [4] performed the parameter estimation for the extraction process of sage oil from seeds and reported $D_i \approx 6e - 13$.

The axial diffusion coefficient obtained from the optimizer seems to be quite high if compared to the internal diffusion coefficients. Nevertheless, the values of D_e^M have similar order of magnitude as reported in literature, for example Reis-Vasco et al. [20]. The relatively high values of the axial diffusion coefficients might be justified by taking into account low values of flow rate used in all the experiments.

The Υ coefficient

As the total amount of the oil present in the system is unknown, and as such it has been obtained from the optimizer. Given the dataset and the process model, the optimizer found that the best fit is obtained if the total mass of the oil reach a lower bound equal to 80 g. The lower bound was estimated by round up of the biggest value of collected cumulative amount of the extraction product. As the same raw material was used in all experiments, the same initial amount of solute is assumed for all the cases.

As explained above, and in Appendix A.6, the linear distribution of can be fully determined if the parameter τ is known. The split ratio for experiments conducted at 40°C / 300 bar and 50°C / 300 bar are similar to each other and close to 0.65. The experiments performed at 40°C / 200 bar and 50°C / 200 bar have τ equals to 0.70 and 0.75, respectively.

The noise present in each dataset is quantified by parameter σ. It can be observed dataset obtained at 40°C / 200 bar and 50°C / 200 bar have similar value of $\sigma \approx 0.36$. The visual investigation of the datasets obtained at 40°C / 300 bar and 50°C / 300 bar allow to explain higher values of σ for both dataset. Both datasets have higher deviation of the data points from the simulated curve.

The results obtained from the parameter estimation are used to develop a generalized process model. The model generalization is performed by introducing correlations which link the estimated parameters and the operating conditions. Since the experiments were performed under varying temperature and pressure, the influence of these variables is taken into account. To simplify the problem, the correlations are written as functions of fluid density rather than temperature and pressure. Since the optimizer found that k_m, m_{total} and C_{lim} don't change with the density variations, they are assumed to be constants and not considered further.

The other two parameters (D_i and D_e^M) are subject to regression to obtain correlations in terms of density. Figure 6 shows the first- and second-order polynomials used to fit D_i and D_e^M as a function of fluid density.

The results of the linear regression applied to D_i and D_e^M are presented in Figure 6a. It can be observed that the internal diffusion coefficient increases with increasing fluid density, while the axial diffusion coefficient decreases.

The increase in the density of the supercritical fluid can lead to an increase in the solubility of the solute and, consequently, an increase in the concentration gradient. This
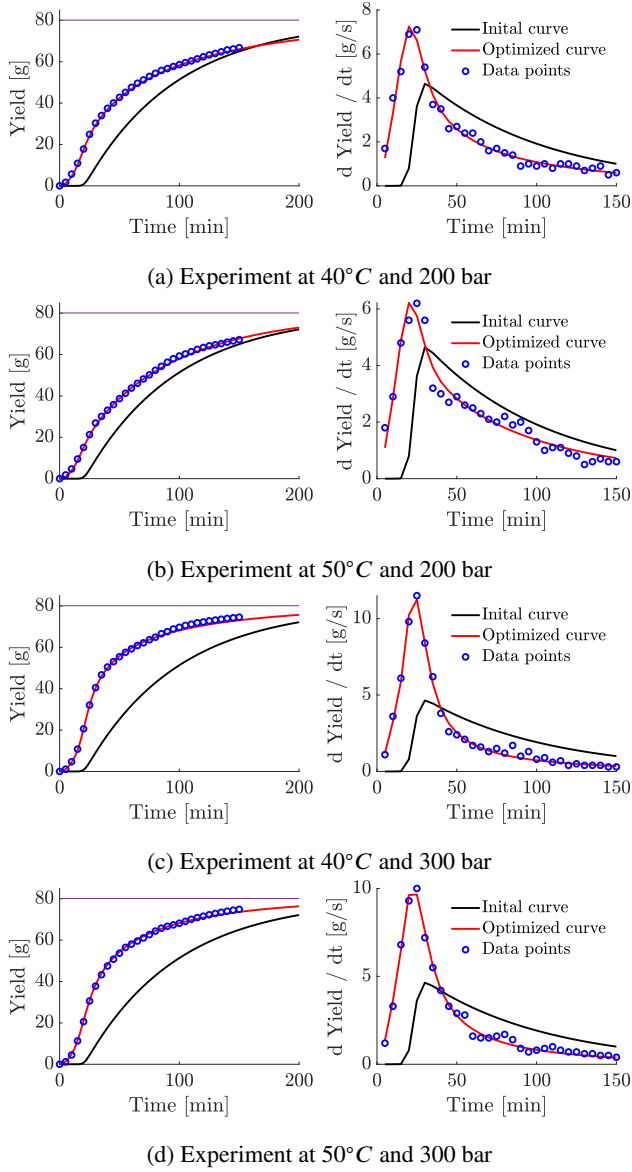
(a) Experiment at 40°C and 200 bar

(b) Experiment at 50°C and 200 bar

(c) Experiment at 40°C and 300 bar

(d) Experiment at 50°C and 300 bar

Figure 5: Results of parameter fitting, with estimation of the initial state

$R^2 = 0.93$
$D_i [m^2/s] \times 1e - 14 = (0.07859)\rho + (-60.43)$

$R^2 = 0.89$
$D_e^M [m^2/s] \times 1e - 6 = (-0.02697)\rho + (29.7)$

(a) First-order polynomial regression of fitted parameters (D_i and D_e^M) as a function of fluid density ρ_f

$R^2 = 1$
$[s] \times 1e - 14 = (0.0005419)\rho^2 + (-0.8611)\rho + (345.3)$

$R^2 = 1$
$D_e^M [m^2/s] \times 1e - 6 = (-0.0002386)\rho^2 + (0.3869)\rho + (-149)$

(b) Second-order polynomial regression of fitted parameters (D_i and D_e^M) as a function of fluid density ρ_f

Figure 6: Regression of D_i and D_e^M

increased concentration gradient drives the solute to diffuse more rapidly through the matrix of the solid particles, resulting in an increased internal mass transfer coefficient. However, the effect of increased solubility on the internal mass transfer coefficient outweighs the resistance from higher density, resulting in an overall increase in the internal mass transfer coefficient with density. The same behaviour can be observed in Figure 5, where plots on the right-hand side exhibit a peak. The higher the peak, the greater the increase in solute concentration in the fluid phase, which can be explained by higher solubility.

The behaviour of the axial diffusion coefficient can be explained through Graham's Law of Diffusion, which states that the rate of diffusion of a molecule is inversely proportional to the square root of its density under given conditions
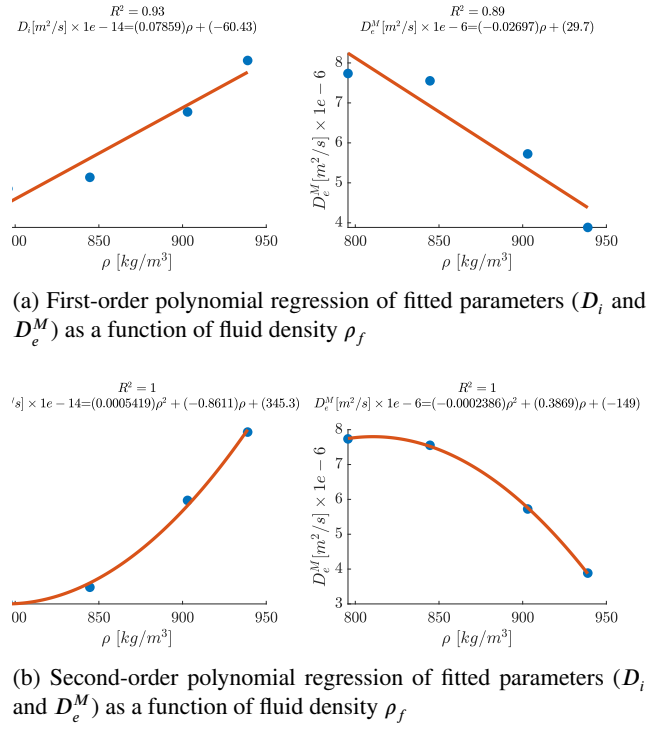
of temperature and pressure. This means that denser media slow down the axial diffusion rate of molecules.

IDEAL I SHOULD SUPPORT THIS EXPLANATION WITH SOME REFERENCES

Figure 6b show the result of fitting a second-order polynomial in density space. It can be observed that the fit obtained from quadratic functions seems to be represent both dataset better.
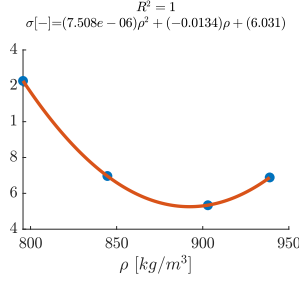
The experimental procedure and the used device can influence the values of τ and σ. Therefore, seeking a general expression for the initial state that is solely a function of operating conditions may not be sufficient to fully describe the relationship between these parameters. However, if first- and second-order regressions are applied to τ and σ, some general conclusions about the trend can be drawn. The results of the regression applied to τ and σ are presented in Figure 7.

As can be seen from Figure 7 , the τ seems to decrease as the fluid density increase. The standard deviation increases as the fluid density increase. As mentioned above, these results should be used with caution due to uninvestigated influence of the equipment on the extraction results.

To prove that the obtained solution is a global solution, the parameter estimation problem was run from multiple initial conditions. The Appendix **??**, contain a solution of the optimization solution and corresponding figures.
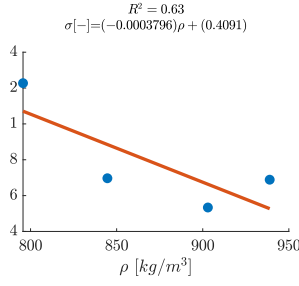
(a) First order polynomial regression of fitted parameters (τ and σ) as a function of fluid density ρ_f

(b) Second order polynomial regression of fitted parameters (τ and σ) as a function of fluid density ρ_f

Figure 7: Regression of τ and σ

The generalized model can be used to study the impact of different operating conditions on the extraction yield or for economic analysis of the extraction process.

4. Conclusions

In this study, a process model was developed by performing parameter estimation using a dataset obtained from experiments conducted at various temperature and pressure levels. The model was found to have good agreement with experimental yield curves for the extraction of caraway oil from caraway seeds. However, it was noticed that the simulation results overshoot the dataset, which may be explained to the presence of losses in the real system, such as some amount of the solute sticking to the inner walls of pipes. Another possible reason could be the need for a more complex mass transfer mechanism than the extraction kinetic presented in this work. For example, the Broken-and-Intact Cell model suggested by Sovova [21] formulated a general SFE model that includes the solute-matrix interaction. This model allows for solute diffusion from intact cells to the region of broken cells, and the equilibrium is established at the particle surface between the broken cells and fluid phase. Such a mechanism gives more flexibility to the process model to adapt to a dataset.

To establish correlations for the internal and axial diffusion coefficients in terms of fluid density, both linear and non-linear regression techniques were utilized. These correlations facilitated the generalization of the process model to a range of operating conditions, specifically for temperatures ranging from $40°C$ to $50°C$, pressures ranging from 200 bar to 300 bar, and flow rates of 0.4 l/min (with flow variations of up to 5%). The dependencies given by these correlations can be justified by the influence of the solubility and Graham's Law of Diffusion, as suggested above.

References

[1] Nevena M. Hromis, Vera L. Lazic, Sinisa L. Markov, Zuzana G. Vastag, Senka Z. Popovic, Danijela Z. Suput, Natalija R. Dzinic, Aleksandra S. Velicanski, and Ljiljana M. Popovic. Optimization of chitosan biofilm properties by addition of caraway essential oil and beeswax. Journal of Food Engineering, 158:86–93, aug 2015. doi: 10.1016/j.jfoodeng.2015.01.001.

[2] Ernesto Reverchon, Giorgio Donsi, and Libero Sesti Osseo. Modeling of supercritical fluid extraction from herbaceous matrices. Industrial & Engineering Chemistry Research, 32(11):2721–2726, nov 1993. doi: 10.1021/ie00023a039.

[3] H. Sovova. Rate of the vegetable oil extraction with supercritical co2. modelling of extraction curves. Chemical Engineering Science, 49 (3):409–414, 1994. doi: 10.1016/0009-2509(94)87012-8.

[4] E. Reverchon. Mathematical modeling of supercritical extraction of sage oil. AIChE Journal, 42(6):1765–1771, jun 1996. doi: 10.1002/aic.690420627.

[5] J Elliott. Introductory chemical engineering thermodynamics. Prentice Hall, Upper Saddle River, NJ, 2011. ISBN 9780136068549.

[6] G. G. Simeoni, T. Bryk, F. A. Gorelli, M. Krisch, G. Ruocco, M. Santoro, and T. Scopigno. The widom line as the crossover between liquid-like and gas-like behaviour in supercritical fluids. Nature Physics, 6(7):503–507, jun 2010. doi: 10.1038/nphys1683.

[7] Daniel Banuti. The latent heat of supercritical fluids. Periodica Polytechnica Chemical Engineering, 63(2):270–275, jan 2019. doi: 10.3311/ppch.12871.

[8] W. Sheng, G. J. Chen, and H. C. Lu. Prediction of transport properties of dense gases and liquids by the peng-robinson (PR) equation of state. International Journal of Thermophysics, 10(1):133–144, jan 1989. doi: 10.1007/bf00500714.

[9] Sydney Chapman and T. G. Cowling. The Mathematical Theory of Non-uniform Gases. Cambridge University Press, 1991. ISBN 9780521408448.

[10] A. Fenghour, William A. Wakeham, and V. Vesovic. The viscosity of carbon dioxide. Journal of Physical and Chemical Reference Data, 27 (1):31–44, jan 1998. doi: 10.1063/1.556013.

[11] Arno Laesecke and Chris D. Muzny. Reference correlation for the viscosity of carbon dioxide. Journal of Physical and Chemical Reference Data, 46(1):013107, mar 2017. doi: 10.1063/1.4977429.

[12] M. L. Huber, E. A. Sykioti, M. J. Assael, and R. A. Perkins. Reference correlation of the thermal conductivity of carbon dioxide from the triple point to 1100 k and up to 200 MPa. Journal of Physical and Chemical Reference Data, 45(1):013102, mar 2016. doi: 10.1063/1.4940892.

[13] John D. Anderson. Computational fluid dynamics the basic with applications. McGraw-Hill, 1995. ISBN 9780071132107.

[14] Stefan Schreier. Compressible flow. Wiley, 1982. ISBN 047105691X.

[15] N. R. Bulley, M. Fattori, A. Meisen, and L. Moyls. Supercritical fluid extraction of vegetable oil seeds. Journal of the American Oil Chemists' Society, 61(8):1362–1365, aug 1984. doi: 10.1007/bf02542243.

[16] M. Spiro and M. Kandiah. Extraction of ginger rhizome: partition constants and other equilibrium properties in organic solvents and in supercritical carbon dioxide. International Journal of Food Science & Technology, 25(5):566–575, jun 2007. doi: 10.1111/j.1365-2621.1990.tb01116.x.

[17] Jürgen Gmehling, Michael Kleiber, Bärbel Kolbe, and Jürgen Rarey. Chemical Thermodynamics for Process Simulation. Wiley, mar 2019. doi: 10.1002/9783527809479.

[18] H. Sovova, R. Komers, J. Kucuera, and J. Jezu. Supercritical carbon dioxide extraction of caraway essential oil. Chemical Engineering Science, 49(15):2499–2505, aug 1994. doi: 10.1016/0009-2509(94)e0058-x.

[19] John Mandel. Fitting a straight line to certain types of cumulative data. Journal of the American Statistical Association, 52(280):552–566, dec 1957. doi: 10.1080/01621459.1957.10501413.

[20] E.M.C Reis-Vasco, J.A.P Coelho, A.M.F Palavra, C Marrone, and E Reverchon. Mathematical modelling and simulation of pennyroyal essential oil supercritical extraction. Chemical Engineering Science, 55(15):2917–2922, aug 2000. doi: 10.1016/s0009-2509(99)00561-8.

[21] Helena Sovova. Broken-and-intact cell model for supercritical fluid extraction: Its origin and limits. The Journal of Supercritical Fluids, 129:3–8, nov 2017. doi: 10.1016/j.supflu.2017.02.014.

[22] Ding-Yu Peng and Donald B. Robinson. A new two-constant equation of state. Industrial & Engineering Chemistry Fundamentals, 15(1): 59–64, feb 1976. doi: 10.1021/i160057a011.

[23] R. M. Pratt. Thermodynamic properties involving derivatives: Using the peng-robinson equation of state, chemical engineering education. CHEMICAL ENGINEERING EDUCATION, 35:112–139, 2001. ISSN 0009-2479. URL https://www.tib.eu/de/suchen/id/BLSE%3ARN095457101.

[24] Pierre-Louis Lions. Mathematical Topics in Fluid Mechanics : Volume 1 Incompressible Models. Oxford University Press, 2013. ISBN 9780199679218.

[25] David Mautner Himmelblau. Process analysis by statistical methods, 1970. [by] David M. Himmelblau., Includes bibliographical references.

A. Appendix

A.1. Thermodynamic

A.1.1. Equation of state and properties of the fluid phase

In this study, the influence of real gas effects are introduced through $P(t)v_m(T(t,z),P(t)) = Z(T(t,z),P(t))RT(t,z)$, where v_m represents the molar volume of CO_2, $Z(T(t,z),P(t))$ denotes its compressibility factor, and R is the universal gas constant. The main advantage of using compressibility in calculations is to express it as an explicit function of temperature and pressure. It can be written as a cubic function of the molar volume (of the density). Detail information about Peng-Robinson equation of state can be found in the work of Peng and Robinson [22], Elliott [5] or Pratt [23]. The P-R EOS is presented by Equation 33.

$$P(t) = \frac{RT(t,z)}{v_m(T(t,z),P(t)) - b} - \frac{a^c \alpha(T(t,z))}{v_m(T(t,z),P(t))^2 + 2bv_m(T(t,z),P(t)) - b^2} \tag{33}$$

The Equation 33 can be also written as the third-order given by Equation 34. Numerical methods such as Newton-Raphson can be used to solve the polynomial equation to obtain the compressibility $Z(T(t,z),P(t))$ at given temperature and pressure. Alternatively, the Cardano formula can be used to get the closed form solution of the Equation 34. Further details regarding the Cardano formula can be found in Appendix A.5.

$$Z^3 - (1 - B(T(t,z),P(t)))Z^2 + \left(A(T(t,z),P(t)) - 2B(T(t,z),P(t)) - 3B(T(t,z),P(t))^2\right)Z = 0 \tag{34}$$

where $A(T(t,z),P(t))$ and $B(T(t,z),P(t))$ are functions of time and space defined on the attraction parameter, $a(T(t,z)) = a^c\alpha(T(t,z))$ with $a^c \approx 0.45724 R^2 T_c^2/P_c$, and the repulsion parameter, $b \approx 0.07780 RT_c/P_c$, both functions of the critical temperature T_c and pressure P_c.

$$A(T(t,z),P(t)) = \frac{\alpha(T(t,z))a^c P(t)}{R^2 T^2(t,z)}; \tag{35a}$$

$$B(T(t,z),P(t)) = \frac{bP(t)}{RT(t,z)}. \tag{35b}$$

The quantity $\alpha(T(t,z))$ is a dimensionless correction term that depends on the temperature $T(t,z)$ and a constant κ. The constant κ is given by the formula $\kappa = 0.37464 + 1.54226\omega - 0.26992\omega^2$, where ω is the acentric factor of CO_2 molecules and is equal to 0.239.

In a one-phase region, the fluid is described by one real root corresponding to the gas, liquid or supercritical phase. The gas-liquid mixture is present in the two-phase region, and two roots are found. The biggest root is assigned to the gas phase, and the smallest root corresponds to the liquid phase.

A.1.2. Density of the fluid phase

The density of the fluid phase, denoted by ρ_f, is assumed to be equal to the density of the solvent at a given temperature and pressure. Since the temperature $T(t,z)$ of the fluid phase is a modelled variable, the density can vary both along the bed and in time. Using the definition of compressibility, the following expression for the density can be obtained:

$$\rho_f(T(t,z),P(t)) = \frac{P(t)M_{CO_2}}{RT(t,z)Z(T(t,z),P(t))}, \tag{36}$$

where M_{CO_2} denotes the molar mass of CO_2, and $Z(T(t,z),P(t))$ is the compressibility factor that solves Eq. (34). This means that the density of the fluid depends on both space and time, due to its dependence on temperature and pressure.

A.1.3. Heat capacity of the fluid phase

Following the work of Pratt [23], it is assumed that the specific heat can be obtained as a sum of ideal gas contribution and a residual correction for non-ideal behaviour, as given by Equations 37a and 37b.

$$C_v(T(t,z),P(t)) = C_v^{\mathrm{I}}(T(t,z),P(t)) + C_v^{\mathrm{R}}(T(t,z),P(t)); \tag{37a}$$

$$C_p(T(t,z),P(t)) = \underbrace{C_p^{\mathrm{I}}(T(t,z),P(t))}_{\text{Eq. (38)}} + \underbrace{C_p^{\mathrm{R}}(T(t,z),P(t))}_{\text{Eq. (39)}}. \tag{37b}$$

$C_v(T(t,z),P(t))$ and $C_p(T(t,z),P(t))$ are the specific heat of CO_2 at constant volume and pressure, respectively.

The ideal-gas contribution $C_v^{\mathrm{I}}(T(t,z),P(t))$ and $C_p^{\mathrm{I}}(T(t,z),P(t))$, can be obtained based on heat-capacity data applicable to gases at low pressure. For CO_2, the ideal gas contribution to the specific heat at constant $P(t)$, as function of $T(t,z)$ is given by,

$$C_p^{\mathrm{I}}(T(t,z),P(t)) = C_{P0} + C_{P1}T(t,z) + C_{P2}T^2(t,z) + C_{P3}T^3(t,z) \tag{38}$$

where the coefficients (REF) of the expansion are $C_{P0} = 4.728$, $C_{P1} = 1.75 \times 10^{-3}$, $C_{P2} = -1.34 \times 10^{-5}$, and $C_{P3} = 4.10 \times 10^{-9}$.

The correction term $C_p^{\mathrm{R}}(T(t,z)P(t))$ at constant pressure $P(t)$, can be defined by introducing $C_p^{\mathrm{I}}(T(t,z)) - C_v^{\mathrm{I}}(T(t,z)) = R$ and using the definition of $C_v^{\mathrm{R}}(T(t,z)P(t))$. The general form of the correction term is given by Equation 39

$$C_p^{\mathrm{R}}(T(t,z),P(t)) = \underbrace{C_v^{\mathrm{R}}(T(t,z),P(t))}_{\text{Eq. (43)}}$$
$$+ T(t,z)\underbrace{\left(\frac{\partial P(t)}{\partial T}\right)_{v_m(t,z)}}_{\text{Eq. (42)}} \underbrace{\left(\frac{\partial v_m(T(t,z),P(t))}{\partial T}\right)_{P(t)}}_{\text{Eq. (40)}} - R. \tag{39}$$

For the partial derivative of the volume with respect to temperature $T(t,z)$ at constant pressure $P(t)$, we have

$$\left(\frac{\partial v_m(T(t,z),P(t))}{\partial T}\right)_{P(t)} = \frac{Z(T(t,z),P(t))R}{P(t)}$$
$$+ \frac{RT(t,z)}{P(t)}\underbrace{\left(\frac{\partial Z(T(t,z),P(t))}{\partial T}\right)_{P(t)}}_{\text{Eq. (41)}} \tag{40}$$

with partial derivative of the compressibility factor with respect to temperature $T(t,z)$ at constant pressure $P(t)$

$$\left(\frac{\partial Z(T(t,z),P(t))}{\partial T}\right)_{P(t)} = \left(\frac{\partial \frac{P(t)v_m(T(t,z),P(t))}{RT(t,z)}}{\partial T}\right)_{P(t)} \tag{41}$$

Similarly, for the partial derivative of the pressure with respect to temperature at constant volume is :

$$\left(\frac{\partial P(t)}{\partial T}\right)_{v_m(t,z)} = \left(\frac{\partial \frac{Z\,RT(t,z)}{v_m(T(t,z),P(t))}}{\partial T}\right)_{v_m(t,z)} \tag{42}$$

The residual specific heat at constant volume is obtained, by definition, by using the residual internal energy

$$C_v^R\left(T(t,z),P(t)\right) = \left(\frac{\partial U^R\left(T(t,z),P(t)\right)}{\partial T}\right)_{v_m(t,z)} \tag{43}$$

A.1.4. Departure functions for enthalpy calculations

In thermodynamics, a departure function is a concept used to calculate the difference between a real fluid's thermodynamic properties and those of an ideal gas, given a specific temperature and pressure. Common departure functions include those for enthalpy, entropy, and internal energy. These functions are used to calculate extensive properties, which are properties computed as a difference between two states.

For example, to evaluate the enthalpy change between two points, $h(V_1, T_1)$ and $h(V_2, T_2)$, we first calculate the enthalpy departure function between the initial volume V_1 and infinite volume at temperature T_1. We then add to that the ideal gas enthalpy change due to the temperature change from T_1 to T_2, and finally subtract the departure function value between the final volume V_2 and infinite volume.

Departure functions are computed by integrating a function that depends on an equation of state and its derivative. The general form of the enthalpy equation is given by:

$$\frac{h^{id} - h}{RT} = \int_{v_m}^{\infty} \left(T\left(\frac{\partial Z}{\partial T}\right)_{v_m}\right)\frac{dv_m}{v_m} + 1 - Z \tag{44}$$

Here, h^{id} represents the enthalpy of an ideal gas, h is the enthalpy of a real fluid, R is the universal gas constant, T is temperature, v_m is the molar volume, and Z is the compressibility factor.

The integral in the equation is evaluated over the range of molar volumes from v_m to infinity. The integral includes a term that depends on the derivative of the compressibility factor with respect to temperature, evaluated at the molar volume v_m. Finally, the term $1 - Z$ is added to account for the deviation of the fluid's properties from those of an ideal gas.

The Peng–Robinson equation of state relates the three interdependent state properties pressure P, temperature T, and molar volume v_m. From the state properties (P, v_m, T), one may compute the departure function for enthalpy per mole (denoted h) as presented by Gmehling et al. [17] or Elliott [5]:

$$h - h^{id} = RT\left(T_r(Z - 1) - 2.078(1 + \kappa)\sqrt{\alpha}\ln\left(\frac{Z + 2.414B}{Z - 0.414B}\right)\right) \tag{45}$$

A.2. Governing equations
A.2.1. Mass continuity

Following the work of Anderson [13], the governing equations for compressible fluid with non-uniform cross-section can be obtained. Let's assume that any properties of the flow are uniform across any given cross-section of an extractor. The variation of the cross-section might result from the partial filling of an extractor or its irregular shape. In reality, such a flow is two-dimensional because the area changes as a function of z, and there is a flow-field variation in both directions. The assumption of quasi-one-dimensional flow dictates that the flow properties are a function of z only. The equations described by quasi-one-dimensional assumption hold: (1) mass conservation, (2) Newton's second law, and (3) energy conservation. The modified governing equation can be derived to ensure that these physical principles are satisfied. Let's start with the integral form of the continuity equation:

$$\frac{\partial}{\partial t}\iiint_{\mathcal{V}_f} \rho_f\, d\mathcal{V}_f + \iint_S \rho_f \mathbf{V}\cdot d\mathbf{S} = 0 \tag{46}$$

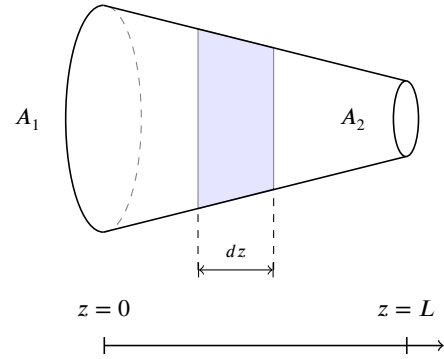We apply this equation to the shaded control volume shown in Fig. 8.

Figure 8: Control volume for deriving the partial differential equation for unsteady, quasi-one-dimensional flow

This control volume is a slice of an extractor, where the infinitesimal thickness of the slice is dz. On the left side of the control volume, consistent with the quasi-one-dimensional assumptions, the density, velocity, pressure, and internal energy denoted by ρ_f, v, P, and e, respectively, are uniform over the area A. Similarly, on the right side of the control volume, the density, velocity, pressure, and internal energy $\rho_f + d\rho_f$, $v + dv$, $P + dP$, and $e + de$, respectively, are uniform over the area available for fluid phase $A_f + dA_f$. Applied to the control volume in Fig. 8, the volume integral in Eq. 46 becomes, in the limit as dz becomes very small,

$$\frac{\partial}{\partial t}\iiint_{\mathcal{V}_f} \rho_f\, d\mathcal{V}_f = \frac{\partial}{\partial t}\left(\rho_f A_f dz\right) \tag{47}$$

where $A\,dz$ is the volume of the control volume in the limit of dz becoming vanishingly small. The surface integral in Eq. 46 becomes

$$\iint_S \rho_f \mathbf{V}\cdot d\mathbf{S} = -\rho_f v A_f + (\rho_f + d\rho_f)(v + dv)(A_f + dA_f) \tag{48}$$

The minus sign on the leading term on the right-hand side is due to the vectors $\mathbf{V}$ and $d\mathbf{S}$ pointing in opposite directions over the left of the control volume, and hence the dot product is negative. Expanding the triple product term

$$\iint_S \rho_f \mathbf{V}\cdot d\mathbf{S} = -\rho_f v A_f + \rho_f v A_f + \rho_f v dA_f + \rho_f A_f dv$$

$$+ \rho_f dv dA_f + v A_f d\rho_f + v d\rho_f dA + A_f d\rho_f dv + d\rho_f dv dA_f \tag{49}$$

In the limit as dz becomes very small, the terms involving products of the differential in Eq. 49, such as $\rho_f dv dA_f$, $d\rho_f dv dA_f$, go to zero much faster than those terms involving only one differential. Hence, all terms involving products of differentials can be dropped, yielding in the limit as dz becomes very small

$$\iint_S \rho_f \mathbf{V} \cdot \mathbf{dS} = \rho_f v dA_f + \rho_f A_f dv + v A_f d\rho_f \tag{50}$$

Substituting Eqs. 47 and 50 into 46, we have

$$\frac{\partial (\rho_f A_f)}{\partial t} + \frac{\partial (\rho_f A_f v)}{\partial z} = 0 \tag{51}$$

The above partial differential equation form of the continuity equation is suitable for unsteady, quasi-one-dimensional flow. It ensures that mass is conserved for this mode of flow. The $A_f(z)$ is an arbitrary function that describes a change in the cross-section of an extractor. The function $A_f(z)$ can be defined as $A_f(z) = \mathbf{A}\phi(z)$, where ϕ is the bed porosity and $\mathbf{A}$ is the cross-section of an empty extractor.

$$\frac{\partial (\rho_f \mathbf{A}\phi(z))}{\partial t} + \frac{\partial (\rho_f \mathbf{A}\phi(z)v)}{\partial z} = 0 \tag{52}$$

The equation can be simplified by canceling out a constant $\mathbf{A}$

$$\frac{\partial (\rho_f \phi(z))}{\partial t} + \frac{\partial (\rho_f \phi(z)v)}{\partial z} = 0 \tag{53}$$

If so-called superficial velocity is defined as $u = \phi v$, the mass continuity becomes

$$\frac{\partial (\rho_f \phi(z))}{\partial t} + \frac{\partial (\rho_f u)}{\partial z} = 0 \tag{54}$$

A.2.2. Transport of a species

The transport of a chemical species, in this case, a solute, can be described by an analogous equation to the Eq. 46 with additional terms on the right-hand side. The first term on the right-hand side describes that a substance goes from high-density regions to low-density regions and is based on the Fick's law $\left(J_{diff} = D_e^M \frac{\partial c_f}{\partial z} \right)$. The other term corresponds to the mass transfer between solid and fluid phases, which is treated as a source term.

$$\frac{\partial}{\partial t} \iiint_{\mathcal{V}_f} c_f d\mathcal{V}_f + \iint_S c_f \mathbf{V} \cdot \mathbf{dS} = \iint_S J_{diff} \cdot \mathbf{n} \, dS + \frac{\partial}{\partial t} \iiint_{\mathcal{V}_s} c_s d\mathcal{V}_s \tag{55}$$

Similarly to the continuity equation, in the limit as dz becomes very small

$$\frac{\partial}{\partial t} \iiint_{\mathcal{V}_f} c_f d\mathcal{V}_f = \frac{\partial}{\partial t} (c_f A_f dz) \tag{56}$$

$$\frac{\partial}{\partial t} \iiint_{\mathcal{V}_s} c_s d\mathcal{V}_s = \frac{\partial}{\partial t} (c_s A_s dz) \tag{57}$$

The surface integrals in the limit of dz become

$$\iint_S c_f \mathbf{V} \cdot \mathbf{dS} = c_f v dA_f + c_f A_f dv + v A_f dc_f \tag{58}$$

From the Divergence theorem in multi-variable calculus, we have

$$\iint_S J_{diff} \cdot \mathbf{n} \, dS = \iiint_{\mathcal{V}_f} \nabla J_{diff} dv_f = \nabla \iiint_{\mathcal{V}_f} J_{diff} dv_f = \nabla \left(J_{diff} A_f dz \right) \tag{59}$$

By substituting the equations derived above into Eq. 55 we obtain

$$\frac{\partial (c_f A_f)}{\partial t} + \frac{\partial (c_f A_f v)}{\partial z} = \frac{\partial (c_s A_s)}{\partial t} + \frac{\partial (J_{diff} A_f)}{\partial z} \tag{60}$$

By defining $A_f = A \cdot \phi$, $A_s = A \cdot (1 - \phi)$ and $u = V \cdot \phi$, and assuming that A is constant, the above equation becomes

$$\frac{\partial (c_f \phi)}{\partial t} + \frac{\partial (c_f u)}{\partial z} = \frac{\partial (c_s(1-\phi))}{\partial t} + \frac{\partial (J_{diff} \phi)}{\partial z} \tag{61}$$

By assuming that $\frac{\partial \phi}{\partial t} = 0$ and expanding J_{diff}, we get

$$\frac{\partial c_f}{\partial t} + \frac{1}{\phi} \frac{\partial (c_f u)}{\partial z} = \frac{(1-\phi)}{\phi} \frac{\partial c_s}{\partial t} + \frac{1}{\phi} \frac{\partial}{\partial z} \left(D_e^M \frac{\partial c_f}{\partial z} \right) \tag{62}$$

The equation can be further simplified if $\frac{\partial u}{\partial z} = \frac{\partial \phi}{\partial z} = D_e^M = 0$, which corresponds to the assumptions of constant velocity along the bed(which might be a case of isothermal and low-Mach number flow), constant porosity(which comes from the assumption of constant area for both solid and fluid phase) and no radial diffusion.

$$\frac{\partial c_f}{\partial t} + \frac{u}{\phi} \frac{\partial c_f}{\partial z} = \frac{1-\phi}{\phi} \frac{\partial c_s}{\partial t} \tag{63}$$

The Eq. 63 is equivalent to the equation presented by Reverchon [4].

A.2.3. Momentum conservation

Similarly to mass conservation, momentum conservation is derived for inviscid fluid with no body forces

$$\frac{\partial}{\partial t} \iiint_{\mathcal{V}_f} (\rho_f v_z) \, d\mathcal{V}_f + \iint_S (\rho_f v_z \mathbf{V}) \, \mathbf{dS} = \iint_S (PdS)_z \tag{64}$$

where V_z is the z component of the velocity.

We the momentum conservation to the shaded control volume in Fig. 8, the integrals on the left side are evaluated in the same manner as discussed above in the regard to the continuity equation. That is,

$$\frac{\partial}{\partial t} \iiint_{\mathcal{V}_f} (\rho_f v_z) \, d\mathcal{V}_f = \frac{\partial}{\partial t} (\rho_f v A_f dz) \tag{65}$$

equation

and

$$\iint_S (\rho_f v_z \mathbf{V}) \, dS = -\rho_f v^2 + (\rho_f + d\rho_f)(v + dv)^2 (A + dA) \tag{66}$$

The evaluation of the pressure force term on the right side of Eq. 64 can be understood based on the Fig. 9. Here, the z components of the vector PdS are shown on all four sides of the control volume. Remember that $\mathbf{dS}$ is assumed to point away from the control volume; hence any z component $(PdS)_z$ that acts toward the left (in the negative z direction) is a negative quantity. Any z component that acts toward the right (in the positive z direction) is a positive quantity. Also note that the z component of PdS acting on the top and the bottom inclined faces of the control volume in Fig. 9 can be expressed as the pressure P acting on the component of the inclined is projected perpendicular to the z direction,
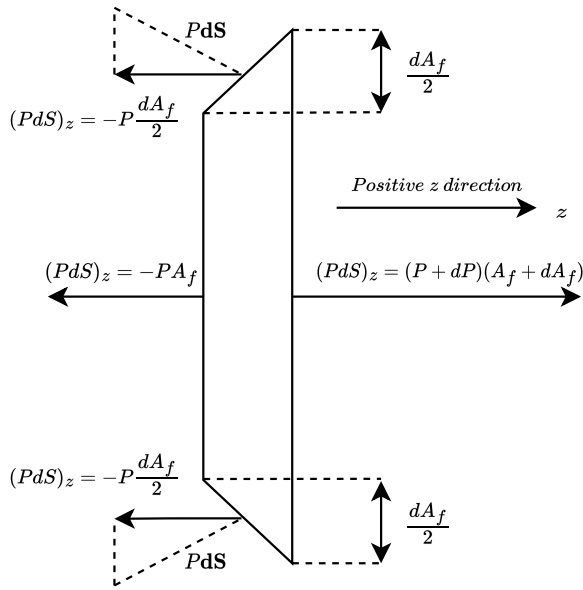
Figure 9: The forces in the z direction acting on the control volume

$dA_f/2$; hence, the contribution of each inclined face (top or bottom) to the pressure integral in Eq. 64 is $-P(dA_f/2)$. All together, the right-hand side of Eq. 64 is expressed as follows:

$$\iint (PdS)_z = -PA_f + (P+dP)(A+dA_f) - 2P\frac{dA_f}{2} \quad (67)$$

Substituting Eqs. 65 to 67 into Eq. 64, we have

$$\frac{\partial}{\partial t}\left(\rho_f v A_f dz\right) - \rho_f v^2 A_f + (\rho_f + d\rho_f)(v+dv)^2(A_f + dA_f)$$
$$= PA_f - (P+dP)(A+dA_f) + PdA_f \quad (68)$$

Canceling like terms and ignoring products of differentials, the equation above becomes in the limit dz becoming very small

$$\frac{\partial}{\partial t}\left(\rho_f v A_f dz\right) + d\left(\rho_f v^2 A_f\right) = -AdP \quad (69)$$

Dividing the above equation by dz and taking the limit as dz goes to zero, we obtain

$$\frac{\partial\left(\rho_f v A_f\right)}{\partial t} + \frac{\partial\left(\rho_f v^2 A_f\right)}{\partial z} = -A_f\frac{\partial P}{\partial z} \quad (70)$$

The Eq. 70 can be expanded further by assuming that $A_f = \mathbf{A}\phi$

$$\frac{\partial\left(\rho_f v \mathbf{A}\phi\right)}{\partial t} + \frac{\partial\left(\rho_f v^2 \mathbf{A}\phi\right)}{\partial z} = -\mathbf{A}\phi\frac{\partial P}{\partial t} \quad (71)$$

The equation can be further simplified by assuming that the cross-section of an extractor $\mathbf{A}$ is constant and cancel out

$$\frac{\partial\left(\rho_f v\phi\right)}{\partial t} + \frac{\partial\left(\rho_f v^2\phi\right)}{\partial z} = -\phi\frac{\partial P}{\partial t} \quad (72)$$

If the superficial velocity $u = \phi V$ is introduced, then the momentum conservation becomes

$$\frac{\partial\left(\rho_f u\right)}{\partial z} + \frac{\partial\left(\rho_f u^2/\phi\right)}{\partial z} = -\phi\frac{\partial P}{\partial z} \quad (73)$$

Eq. 70 represents the conservative form of the momentum equation for the quasi-one-dimensional flow. The equivalent non-conservative form can be obtained by multiplying the continuity equation by v and subtracting it from Eq. 70

$$\frac{\partial\left(\rho_f v A_f\right)}{\partial t} - V\frac{\partial\left(\rho_f A_f\right)}{\partial t} + \frac{\left(\rho_f v^2 A_f\right)}{\partial z} - V\frac{\left(\rho_f v A_f\right)}{\partial z} = -A_f\frac{\partial P}{\partial z} \quad (74)$$

Expanding the derivatives on the left-hand side of the above equation and canceling like terms, gives

$$\rho_f A_f\frac{\partial v}{\partial t} + \rho_f A_f v\frac{\partial v}{\partial z} = -A_f\frac{\partial P}{\partial z} \quad (75)$$

Dividing the above equation by A_f the non-conservative form of the momentum can be obtained

$$\rho_f\frac{\partial v}{\partial t} + \rho_f v\frac{\partial v}{\partial z} = -\frac{\partial P}{\partial z} \quad (76)$$

The Eq. 76 is stylistically the same as the general momentum conservation for one-dimensional flow with no-body forces. The momentum equation can be expressed in terms of superficial velocity $u = v\phi$.

$$\rho_f\frac{\partial (u/\phi)}{\partial t} + \rho_f\frac{u}{\phi}\frac{\partial (u/\phi)}{\partial z} = -\frac{\partial P}{\partial z} \quad (77)$$

By expanding all the terms of the equation above, we get

$$\frac{\rho_f}{\phi}\frac{\partial u}{\partial t} + \rho_f u\frac{\partial\phi^{-1}}{\partial t} + \rho_f\frac{u}{\phi}\frac{1}{\phi}\frac{\partial u}{\partial z} + \rho_f\frac{u}{\phi}u\frac{\partial\phi^{-1}}{\partial z} = -\frac{\partial P}{\partial z} \quad (78)$$

If the bed is not compressible and doesn't change its properties during the batch, then $\dfrac{\partial\phi}{\partial t} = 0$

$$\frac{\rho_f}{\phi}\left(\frac{\partial u}{\partial t} + \frac{u}{\phi}\frac{\partial u}{\partial z} + u^2\frac{\partial\phi^{-1}}{\partial z}\right) = -\frac{\partial P}{\partial z} \quad (79)$$

If the porosity is constant along an extractor, then the momentum conservation equation becomes

$$\frac{\rho_f}{\phi}\left(\frac{\partial u}{\partial t} + \frac{u}{\phi}\frac{\partial u}{\partial z}\right) = -\frac{\partial P}{\partial z} \quad (80)$$

The Eq. 80 represents the non-conservative form of the momentum equation for quasi-one-dimensional flow with no body forces and constant porosity.

A.2.4. Energy conservation

Let's consider the integral form of the energy equation for adiabatic flow with no body forces and no viscous effects

$$\frac{\partial}{\partial}\iiint_{V_f}\rho_f\left(e_f + \frac{v^2}{2}\right)dV_f + \iint_S\rho_f\left(e_f + \frac{v^2}{2}\right)\mathbf{V}\cdot\mathbf{dS} = -\iint_S (P\mathbf{V})\cdot\mathbf{dS} \quad (81)$$

Applied to the shaded control volume in Fig. 8, and keeping in mind the pressure forces shown in Fig. 9, Eq. 81 becomes

$$\frac{\partial}{\partial t}\left[\rho_f\left(e_f + \frac{v^2}{2}\right)A_f dz\right] - \rho_f\left(e_f + \frac{v^2}{2}\right)vA_f$$
$$+ (\rho_f + d\rho_f)\left[e_f + de_f + \frac{(v+dv)^2}{2}\right](V+dV)\left(A_f + dA_f\right)$$
$$= -\left[-PvA_f + (P+dP)(v+dv)\left(A_f + dA_f\right) - 2\left(Pv\frac{dA_f}{2}\right)\right]$$
$$\quad (82)$$

Neglecting products of differential and canceling like terms, the above equation becomes

$$\frac{\partial}{\partial t}\left[\rho_f\left(e_f + \frac{v^2}{2}\right)A_f dz\right] + d\left(\rho_f r_f A_f\right) + \frac{\left(\rho_f v^3 A_f\right)}{2} = -d\left(PA_f v\right)$$

(83)

or

$$\frac{\partial}{\partial t}\left[\rho_f\left(e_f + \frac{v^2}{2}\right)A_f dz\right] + d\left[\rho_f\left(e_f + \frac{v^2}{2}\right)vA_f\right] = -d\left(PA_f v\right)$$ (84)

Taking the limit as dz approaches zero, the equation above becomes the following partial differential equation

$$\frac{\partial\left[\rho_f\left(e_f + v^2/2\right)A\right]}{\partial t} + \frac{\partial\rho_f\left(e_f + v^2/2\right)vA_f}{\partial z} = -\frac{\partial\left(PA_f v\right)}{\partial z}$$ (85)

Equation 85 is the conservation form of the energy expressed in terms of the total energy $e + v^2/2$, appropriate for unsteady, quasi-one-dimensional flow. The energy equation can be expressed in terms of internal energy if Eq. 70 is multiplicated by v and then subtracted from Eq. 85

$$\frac{\partial\left(\rho_f e_f A_f\right)}{\partial t} + \frac{\partial\left(\rho_f e_f v A_f\right)}{\partial z} = -P\frac{\partial A_f v}{\partial z}$$ (86)

The equation above is the conservation form of the energy equation expressed in terms of internal energy e_f suitable for quasi-one-dimensional flow. The non-conservative for is then obtained by multiplying the continuity equation 51, by e_f and substructing it from 86, yielding

$$\rho_f A_f\frac{\partial e_f}{\partial t} + \rho_f A_f v\frac{\partial e_f}{\partial z} = -P\frac{\partial(A_f v)}{\partial z}$$ (87)

Expanding the right-hand side and dividing by A_f, the above equation becomes

$$\rho_f\frac{\partial e_f}{\partial t} + \rho_f v\frac{\partial e_f}{\partial z} = -P\frac{v}{A_f}\frac{\partial A_f}{\partial z}$$ (88)

or

$$\rho_f\frac{\partial e_f}{\partial t} + \rho_f v\frac{\partial e_f}{\partial z} = -P\frac{\partial v}{\partial z} - PV\frac{\partial(\ln A_f)}{\partial z}$$ (89)

Equation 89 is the non-conservative form of the energy equation expressed in terms of internal energy, appropriate to unsteady quasi-one-dimensional flow. The reason for obtaining the energy equation in the form of Eq. 89 is that, for a calorically perfect gas, it leads directly to a form of the energy equation in terms of temperature T.

A.3. Low Mach number expansion

As discussed by Lions [24], the low Mach number equations are a subset of the fully compressible equations of motion (continuity, momentum and energy). Such a set of equations allow for large variations in gas density, but it is considered acoustically incompressible. Therefore, the low Mach number equations are preferred over the full compressible equations for low-speed flow problems $\left(M_a = \frac{|v|}{\sqrt{\partial P/\partial\rho_f}} \ll 1\right)$ to avoids the need to resolve fast-moving acoustic signals. The equations are derived from

compressible equations based on the perturbation theory. The perturbation theory develops an expression for the desired solution in terms of a formal power series known as a perturbation series in some "small" parameter ζ, that quantifies the deviation from the exactly solvable problem. The leading term in this power series is the solution of the exactly solvable problem, while further terms describe the deviation in the solution due to the deviation from the initial problem.

The Equations 1 to 2 describe the fully compressible equations of motion (respectively, the transport of mass, momentum and energy) for the quasi-one-dimensional case. We rescale the time variable, considering finally

$$\rho_\zeta = \rho\left(z, t/M_a\right), \quad v_\zeta = \frac{1}{\zeta}v\left(z, t/M_a\right)$$

$$T_\zeta = T\left(z, t/M_a\right), \quad k_\zeta = \zeta k(\rho_f, T)$$

The conservative non-dimensional equations of motion become

$$\frac{\partial\left(\rho_\zeta A_f\right)}{\partial t} + \frac{\partial\left(\rho_\zeta A_f v_\zeta\right)}{\partial z} = 0$$

$$\frac{\partial\left(\rho_\zeta A_f v_\zeta\right)}{\partial t} + \frac{\partial\left(\rho_\zeta v_\zeta A_f v_\zeta\right)}{\partial z} + \frac{A_f}{M_a^2}\frac{\partial P_\zeta}{\partial z} = 0$$

$$\frac{\partial\left(\rho_\zeta e_\zeta A_f\right)}{\partial t} + \frac{\partial\left(\rho_\zeta e_\zeta v_\zeta A_f\right)}{\partial z} - \frac{\partial}{\partial z}\left(k\frac{\partial T_\zeta}{\partial z}\right) + P_\zeta\frac{\partial\left(A_f v_\zeta\right)}{\partial z} = 0$$

Let's define $\zeta = M_a^2$ and assume small Mach numbers, $M_a \ll 1$, then the kinetic energy, viscous work, and gravity work terms can be neglected in the energy equation since the square of the Mach number scales those terms. The inverse of Mach number squared remains in the momentum equations, suggesting singular behaviour. In order to explore the singularity, the pressure, velocity and temperature are expanded as asymptotic series in terms of the parameter ζ

$$P_\zeta = P_0 + P_1\zeta + P_2\zeta^2 + \mathcal{O}(\zeta^3)$$

$$\rho_\zeta = \rho_0 + \rho_1\zeta + \mathcal{O}(\zeta^2)$$

$$v_\zeta = v_0 + v_1\zeta + \mathcal{O}(\zeta^2)$$

$$T_\zeta = T_0 + T_1\zeta + \mathcal{O}(\zeta^2)$$

$$e_\zeta = e_0 + e_1\zeta + \mathcal{O}(\zeta^2)$$

By expanding performing power expansion on the continuity equation and taking the limit of ζ from the positive side, we get

$$\lim_{\zeta\to 0_+}\frac{\partial\left(\left(\rho_0 + \rho_1\zeta + \mathcal{O}(\zeta^2)\right)A_f\right)}{\partial t} +$$

$$+ \frac{\partial\left(\left(\rho_0 + \rho_1\zeta + \mathcal{O}(\zeta^2)\right)A_f\left(v_0 + v_1\zeta + \mathcal{O}(\zeta^2)\right)\right)}{\partial z} = 0$$

The continuity equation becomes

$$\frac{\partial\left(\rho_0 A_f\right)}{\partial t} + \frac{\partial\left(\rho_0 A_f v_0\right)}{\partial z} = 0$$ (90)

The form of the continuity equation stays the same. Considering the momentum equation, it can be seen that the inverse of Mach number squared remains, which suggests singular behaviour.

$$\lim_{\zeta \to 0_+} \frac{\partial \left(\left(\rho_0 + \rho_1\zeta + \mathcal{O}(\zeta^2)\right) A_f \left(v_0 + v_1\zeta + \mathcal{O}(\zeta^2)\right)\right)}{\partial t} +$$

$$+ \frac{\partial \left(\left(\rho_0 + \rho_1\zeta + \mathcal{O}(\zeta^2)\right) A_f \left(v_0 + v_1\zeta + \mathcal{O}(\zeta^2)\right)\left(v_0 + v_1\zeta + \mathcal{O}(\zeta^2)\right)\right)}{\partial z} +$$

$$+ A_f \frac{\partial}{\partial z}\left(\frac{P_0}{M_a^2} + \frac{P_1\zeta}{M_a^2} + \frac{P_2\zeta^2}{M_a^2} + \mathcal{O}(\zeta^3)\right)$$

The first two terms stay the same, but the third one becomes different in structure. By further investigation of the pressure term in the momentum equation, it can be observed.

$$\lim_{\zeta \to 0_+} \frac{\partial}{\partial z}\left(\frac{P_0}{M_a^2} + \frac{P_1\zeta}{M_a^2} + \frac{P_2\zeta^2}{M_a^2} + \mathcal{O}(\zeta^3)\right) =$$

$$= \lim_{\zeta \to 0_+} \frac{\partial}{\partial z}\left(\frac{P_0}{M_a^2}\right) + \frac{\partial}{\partial z}\left(\frac{P_1\zeta^2}{M_a^2}\right) + \frac{\partial}{\partial z}\left(\frac{P_2\zeta^2}{M_a^2}\right)$$

$$= \lim_{\zeta = M_a^2 \to 0_+} \frac{\partial}{\partial z}\left(\frac{P_0}{M_a^2}\right) + \frac{\partial}{\partial z}\left(\frac{P_1 M_a^2}{M_a^2}\right) + \frac{\partial}{\partial z}\left(\frac{P_2 M_a^4}{M_a^2}\right)$$

$$= \lim_{\zeta = M_a^2 \to 0_+} 0 + \frac{\partial P_1}{\partial z} + 0$$

The simplification of the P_0 in the momentum equation comes from the fact that P_0 is independent of z. As was presented above, the thermodynamical pressure moves with the speed of sound, and any perturbation propagates instantaneously. The term related to P_2 and higher order terms become zero at the limit of $M_a \to 0$. The momentum equation becomes

$$\frac{\partial (\rho_0 A_f v_0)}{\partial t} + \frac{\partial (\rho_0 v_0 A_f v_0)}{\partial z} + A_f \frac{\partial P_1}{\partial z} = 0$$

By expanding performing power expansion on the energy equation and taking the limit of ζ from the positive side, we get

$$\lim_{\zeta \to 0_+} \frac{\partial \left(\left(\rho_0 + \rho_1\zeta + \mathcal{O}(\zeta^2)\right) A_f \left(e_0 + e_1\zeta + \mathcal{O}(\zeta^2)\right)\right)}{\partial t} +$$

$$+ \frac{\partial \left(\left(\rho_0 + \rho_1\zeta + \mathcal{O}(\zeta^2)\right) A_f \left(v_0 + v_1\zeta + \mathcal{O}(\zeta^2)\right)\left(e_0 + e_1\zeta + \mathcal{O}(\zeta^2)\right)\right)}{\partial z} +$$

$$+ \frac{\partial}{\partial z}\left(k\frac{\partial}{\partial z}\left(T_0 + T_1\zeta + \mathcal{O}(\zeta^2)\right)\right) +$$

$$- \left(P_0 + P_1\zeta + P_2\zeta^2 + \mathcal{O}(\zeta^3)\right) \frac{\partial \left(A_f \left(v_0 + v_1\zeta + \mathcal{O}(\zeta^2)\right)\right)}{\partial z} = 0$$

The form of the energy equation stays the same.

$$\frac{\partial (\rho_0 e_0 A_f)}{\partial t} + \frac{\partial (\rho_0 e_0 v_0 A_f)}{\partial z} - \frac{\partial}{\partial z}\left(k\frac{\partial T_0}{\partial z}\right) + P_0 \frac{\partial (A_f v_0)}{\partial z} = 0$$

where $e_0 = e(\rho_0, T_0)$ and $k = k(\rho_0, T_0)$.

The expansion results in two different types of pressure and they are considered to be split into a thermodynamic component (P_0) and a dynamic component (P_1). The thermodynamic pressure is constant in space, but can change in time. The thermodynamic pressure is used in the equation of state. The dynamic pressure only arises as a gradient term in the momentum equation and acts to enforce continuity.

The resulting unscaled low Mach number equations are:

$$\frac{\partial (\rho_f A_f)}{\partial t} + \frac{\partial (\rho_f A_f v)}{\partial z} = 0$$

$$\frac{\partial (\rho_f A_f v)}{\partial t} + \frac{\partial (\rho_f v A_f v)}{\partial z} + A_f \frac{\partial P_1}{\partial z} = 0$$

$$\frac{\partial (\rho_f e A_f)}{\partial t} + \frac{\partial (\rho_f e v A_f)}{\partial z} - \frac{\partial}{\partial z}\left(k\frac{\partial T}{\partial z}\right) + P_0 \frac{\partial (A_f v)}{\partial z} = 0$$

The energy equation can be expanded through the chain rule to obtain

$$\rho A_f\left(\frac{\partial e}{\partial t} + v\frac{\partial e}{\partial z}\right) + e\underbrace{\left(\frac{\partial (\rho_f A_f)}{\partial t} + \frac{\partial (\rho_f v A_f)}{\partial z}\right)}_{Continutiy} - \frac{\partial}{\partial z}\left(k\frac{\partial T}{\partial z}\right) + P_0 \frac{\partial (A_f v)}{\partial z} = 0$$

The non-conservative form of the energy equation becomes

$$\rho A_f\left(\frac{\partial e}{\partial t} + v\frac{\partial e}{\partial z}\right) - \frac{\partial}{\partial z}\left(k\frac{\partial T}{\partial z}\right) + P_0 \frac{\partial (A_f v)}{\partial z} = 0$$

If the calorically perfect gas is assumed, then $e = C_v T$, where C_v is the constant specific heat. The energy equation can be derived in terms of temperature T.

$$\rho A_f C_v\left(\frac{\partial T}{\partial t} + v\frac{\partial T}{\partial z}\right) - \frac{\partial}{\partial z}\left(k\frac{\partial T}{\partial z}\right) + P_0 \frac{\partial (A_f v)}{\partial z} = 0$$

If an isothermal case is assumed, then the energy equation becomes

$$\lim_{\Delta T \to 0_+} \rho A_f C_v\left(\frac{\partial T}{\partial t} + v\frac{\partial T}{\partial z}\right) - \frac{\partial}{\partial z}\left(k\frac{\partial T}{\partial z}\right) + P_0 \frac{\partial (A_f v)}{\partial z} = 0$$

which leads to

$$\frac{\partial (A_f v)}{\partial z} = 0 \tag{91}$$

In one-dimensional case, the Equation 91 become equivalent of $\text{div}(A_f v) = 0$, which known as the incompressibility condition (Lions [24]).

As presented by Elliott [5], a general formulation of the internal energy for a real gas is:

$$de = C_v dT - \left[P - T\left(\frac{\partial P}{\partial T}\right)_{v_m}\right] dv_m$$

where v_m is the molar volume.

The internal energy is a function of two intensive properties, in this case, T and $v_m = 1/\rho_f$. But, in the case of an ideal gas, the equation of state is such that the second term in this equation is identically equal to zero. So the ideal gas is a special case in which the molar internal energy is a function only of temperature. For Peng-Robinson equation of state, the internal energy is defined as

$$e = C_v T + \frac{a\left(\alpha - T\frac{d\alpha}{dT}\right)}{2\sqrt{2}b} \ln\left[\frac{1 + b\left(1 - \sqrt{2}\rho\right)}{1 + b\left(1 + \sqrt{2}\rho\right)}\right]$$

Assuming constant temperature and pressure along space and in time:

$$\lim_{\Delta T, \Delta P \to 0_+} \rho A_f\left(\frac{\partial e}{\partial t} + v\frac{\partial e}{\partial z}\right) - \frac{\partial}{\partial z}\left(k\frac{\partial T}{\partial z}\right) + P_0\frac{\partial (A_f v)}{\partial z} = 0 \to \frac{\partial (A_f v)}{\partial z} = 0$$

It can be deduced that the continuity equation becomes $\frac{\partial \rho_f}{\partial t} = 0$ at constant temperature and pressure. Moreover, the incompressibility condition $div(A_f v) = 0$ is obtained.

Assuming an arbitrary function $\hat{P}$, which describes the total pressure, the dimensional momentum equation can be written as

$$V \underbrace{\left(\frac{\partial (\rho_f A_f)}{\partial t} + \frac{(\rho_f v A_f)}{\partial z} \right)}_{Continuity\ equation} + \rho_f A_f \frac{\partial v}{\partial t} + \rho_f v A_f \frac{\partial v}{\partial z} = -A_f \frac{\partial \hat{P}}{\partial z}$$

From the incompressibility conditions, we can deduce that

$$\frac{\partial (A_f v)}{\partial z} = 0 \rightarrow A_f \frac{\partial v}{\partial z} = -v \frac{\partial A_f}{\partial z}$$

By combining both above equations, assuming that $\partial v / \partial t = 0$:

$$\frac{\rho_f v^2}{A_f} \frac{\partial A_f}{\partial z} = \frac{\partial \hat{P}}{\partial z} \rightarrow \int \frac{\rho_f v^2}{A_f} \frac{\partial A_f}{\partial z} dz = \int \frac{\partial \hat{P}}{\partial z} dz$$

The l.h.s integral can be solved by assuming ρ_f is constant and introducing superficial velocity $u_s = A_f v$

$$\int \frac{\rho_f v^2}{A_f} \frac{\partial A_f}{\partial z} dz = \int \frac{\rho_f v^2}{A_f} \frac{A_f^2}{A_f^2} \frac{\partial A_f}{\partial z} dz$$

$$= \rho_f u_s^2 \int \frac{1}{A_f^3} \frac{\partial A_f}{\partial z} dz = -\frac{\rho_f u_s^2}{2\Delta A_f^2} = -\frac{\rho_f \Delta v^2}{2}$$

$$\int \frac{\partial \hat{P}}{\partial z} dz = \Delta \hat{P}$$

The final form of the momentum equation corresponds to Bernoulli's principle

$$\Delta \hat{P} = -\frac{\rho_f \Delta v^2}{2} \xrightarrow{P_0 = const} \Delta M_a^2 P_1 = -\frac{\rho_f \Delta v^2}{2}$$

Bernoulli's principle can be used to find the hydrodynamic pressure caused by varying cross-sections at steady-state. Moreover, if the flow velocity is relatively low, all pressure changes are hydrodynamic (due to velocity motion) rather than thermodynamic. The effect of this is that $\partial \rho / \partial P = 0$. In other words, the small changes in pressure due to flow velocity changes do not change the density. This has a secondary effect – the speed of sound in the fluid is $\partial P / \partial \rho = \infty$ in this instance. So there is an infinite speed of sound, which makes the equations elliptic in nature. It can be deduced that at the isothermal conditions, the density in the system propagates with the same speed as pressure since they are both connected through the equation of state.

A.4. Bayes theorem

As discussed by Himmelblau [25], the Bayesian approach to estimation makes use of prior information. Such prior knowledge can come from theoretical considerations, from the results of previous experiments, or from assumptions by the experimenter. Typically, a Bayesian approach assumes a prior probability distribution of an unknown parameter θ in some parameter space $\boldsymbol{\theta}$. The distribution is updated by using Bayes' rule to obtain the posterior probability distribution.

Consider a set of events or outcomes, $A_1, A_2, ..., A_n$, and some other event B. Bayes' theorem states that the probability that event A_i will occur, given that event, B has already occurred, which will be denoted by $P\{A_i|B\}$, is equal to the product of the probability that A_i will occur regardless of whether B will take place and the probability that B will occur, given that A_i has already taken place, divided by the probability of the occurrence of B:

$$P\{A_i|B\} = \frac{P\{B|A_i\}P\{A_i\}}{P\{B\}} \tag{92}$$

Further, if all events comprising the set $\{A_i\}$ are included in $A_1, A_2, ..., A_n$, then

$$P\{A_i|B\} = \frac{P\{B|A_i\}P\{A_i\}}{\sum_{i=1}^{n} P\{B|A_i\}P\{A_i\}} \tag{93}$$

We can interpret these symbols as follows:

1. $P\{A_i\}$ is a measure of our degree of belief that event A_i will occur or that hypothesis A_i is true prior to the acquisition of additional evidence that may alter the measure. $P\{A_i\}$ is denoted the *prior probability*.

2. $P\{A_i|B\}$ is a measure of our degree of belief that event A_i will occur or that hypothesis A_i is true, given additional evidence B pertinent to the hypothesis. $P\{A_i|B\}$ is termed the *posterior probability*.

3. $P\{B|A_i\}$ denotes the likelihood that event B will occur, given that event A_i is true. $P\{B|A_i\}$ is a conditional probability, interpreted in the Bayesian framework as a likelihood, $L(A_i|B)$.

For a continuous variables, Bayes' theorem can be more conveniently expressed in terms of the probability density function rather than the probabilities themselves. Equation 93 can be expressed in terms of a set of observed values of the random variable X, the experimental data $\mathbf{x}$ and unknown parameter θ as

$$p(\theta|X = \mathbf{x}) = p(\theta|\mathbf{x}) = \frac{L(\theta|\mathbf{x}) p(\theta)}{\int_{-\infty}^{+\infty} L(\theta|\mathbf{x}) p(\theta) d\theta} \tag{94}$$

where
$p(\theta|\mathbf{x}) =$ the posterior probability density function for θ; it includes knowledge of the possible values of θ gained from the experimental data $\mathbf{x}$
$p(\theta) =$ the prior probability density function for θ (before the experiment in which $\mathbf{x}$ was observed)
$L(\theta|\mathbf{x}) = p(\mathbf{x}|\theta) =$ the probability density function termed the likelihood function of θ given $\mathbf{x}$

The denominator in Equation 94 is a normalizing factor chosen so that the integration of the posterior distribution is unit, i.e., $\int_{-\infty}^{+\infty} p(\theta|\mathbf{x}) = 1$. By taking into account the law of total probability, the denominator can be written as

$$\int_{-\infty}^{+\infty} p(\mathbf{x}|\theta) p(\theta) d\theta = p(\mathbf{x}) \tag{95}$$

If the prior distribution is a uniform distribution, that is the prior distribution is a constant, the Equation 94 reduces to

$$p(\theta|\mathbf{x}) = \frac{L(\theta|\mathbf{x})}{\int_{-\infty}^{+\infty} L(\theta|\mathbf{x})\, d\theta} \tag{96}$$

If the prior knowledge concerning a postulated event or hypothesis is poor, the posterior probability is largely or entirely determined by the likelihood function, that is, by the additional accumulated evidence for which the likelihood function acts as a mathematical expression. If prior knowledge outweighs recent evidence, however, then the posterior probability is determined almost solely by the prior probability.

In the application of tests and the design of experiments, certain definitions and rules concerning probability are needed and are listed below.

1. It follows from the frequency theory of probability that: $0 \leq P \leq 1$

2. If the probability of occurrence of one event A depends on whether or not event B has occurred, the two events are termed *dependent*; if the probability of occurrence of event A does not depend on the occurrence of B or the reverse, the two events are *independent*.

3. **Addition Rule** If $A_1, A_2, ..., A_n$ are mutually exclusive events, i.e., cannot occur at the same time, the probability of occurrence of just one of the events is equal to the sum of the probabilities of each A_i:

$$P(A_1 \text{ or } A_2 ... \text{ or } A_n) = \sum_{i=1}^{n} P(A_i) \tag{97}$$

Very often we let

$$\sum_{i=1}^{n} P(A_i) = 1 \tag{98}$$

Also, if each event is equiprobable so that $P(A_i) = q$,

$$\sum_{i=1}^{n} q = nq = 1 \qquad \text{or} \qquad q = \frac{1}{n} = P(A_i) \tag{99}$$

In set theory, mutually exclusive events have no points in common. The union of the sets which represents the set of all elements that belong to

$$P(A_1 \cup A_2 \cup ... \cup A_n) = P(A_1) + P(A_2) + ... + P(A_n) \tag{100}$$

4. **Multiplication Rule** If A and B are *independent* event

$$P(A \text{ and } B) = P(A)P(B) \tag{101}$$

In set theory the intersection of A and B is the set of all elements that belong to A and B:

$$P(A \cap B) = P(A)P(B) \tag{102}$$

If the A and B are *dependet* events,

$$P(A|B) = \frac{P(A \cap B)}{P(B)} \tag{103}$$

where the symbol $P(A|B)$ means "probability of A given B". As a corollary,

$$P(A \cap B) = P(B)P(A|B) \tag{104a}$$
$$= P(A)P(B|A) \tag{104b}$$

Two kinds of probabilities enter Equation 104a (or Equation 104b): the absolute probability of event B (or A) irrespective of whether or not A (or B) has occurred, and that the conditional probability of event A (or B) computed on the assumption that B (or B) has occurred. Equation 102 or 103 is special case of Equation 104a or 104b, because if the event are independent $P(A|B) = P(A)$. For the case of many event, Equation 102 can be expanded to

$$P(A_1 \text{ and } A_2 \text{ and } ... \text{ and } A_n) = P(A_1) \cdot P(A_2) \cdot ... \cdot P(A_n)$$
$$= \prod_{i=1}^{n} P(A_i) \tag{105}$$

5. Another useful relationship for events that are not mutually exclusive is

$$P(A) + P(B) - P(A \cap B) = P(A \cup B) \tag{106}$$

A.5. Cardano's Formula

Following the work of Gmehling et al. [17], a cubic equation of state can be written a following form

$$Z^3 + UZ^2 + SZ + T = 0 \tag{107}$$

with Z as the compressibility factor. Using Cardano's formula, this type of equation can be solved analytically. With the abbreviations

$$P = \frac{3S - U^2}{3} \qquad Q = \frac{2U^3}{27} - \frac{US}{3} + T$$

the discriminant can be determined to be

$$D = \left(\frac{P}{3}\right)^3 + \left(\frac{Q}{2}\right)^2 \tag{108}$$

For $D > 0$, the equation of state has one real solution:

$$Z = \left[\sqrt{D} - \frac{Q}{2}\right]^{1/3} - \frac{P}{3\left[\sqrt{D} - \frac{Q}{2}\right]^{1/3}} - \frac{U}{3} \tag{109}$$

For $D < 0$, there are three real solutions. With the abbreviations

$$\Theta = \sqrt{-\frac{P^3}{27}} \qquad \Phi = \arccos\left(\frac{-Q}{2\Theta}\right)$$

they can be written as

$$Z_1 = 2\Theta^{(1/3)} \cos\left(\frac{\Phi}{3}\right) - \frac{U}{3} \tag{110}$$

$$Z_2 = 2\Theta^{(1/3)} \cos\left(\frac{\Phi}{3} + \frac{2\pi}{3}\right) - \frac{U}{3} \tag{111}$$

$$Z_3 = 2\Theta^{(1/3)} \cos\left(\frac{\Phi}{3} + \frac{4\pi}{3}\right) - \frac{U}{3} \tag{112}$$

The largest and the smallest of the three values correspond to the vapor and to the liquid solutions, respectively. The middle one has no physical meaning.

A.6. Initial and boundary conditions

It is assumed that the solvent is free of solute at the entrance of the extractor and that all the solid particles have the same initial solute content c_s^0. It is considered that the initial temperature of the extractor in every place is the same and described by h^0.

During the preparation period, when the operating conditions are achieved, the solute diffuses to the fluid phase in contact with the solid particles. Later, the solute in the fluid phase is partially moved (if the pressure increase in the system, the pump cause the movement of the fluid, even if the outlet valve is closed) to the region where there is no solid phase. As a result, the distribution of solutes mass in the fluid phase is assumed to not be uniform, and described by an arbitrary function $H = H(z)$. Some conclusions can be drawn from the analysis of the initial part of each yield curve. It can be noticed that each curve at the beginning has a curvature, which is not linear. In a general sense, it can be said that a quadratic function could approximate the initial part of each extraction curve. A function that, after integration, gives a quadratic-like result is a straight line. Based on that observation, the solute concentration in the fluid phase is assumed to be linearly distributed. The solute concentration is assumed to be zero at the outlet and reach the maximum at the beginning of the fixed bed. The graphical representation of the solute concentration in the fluid phase is shown in Figure 10.
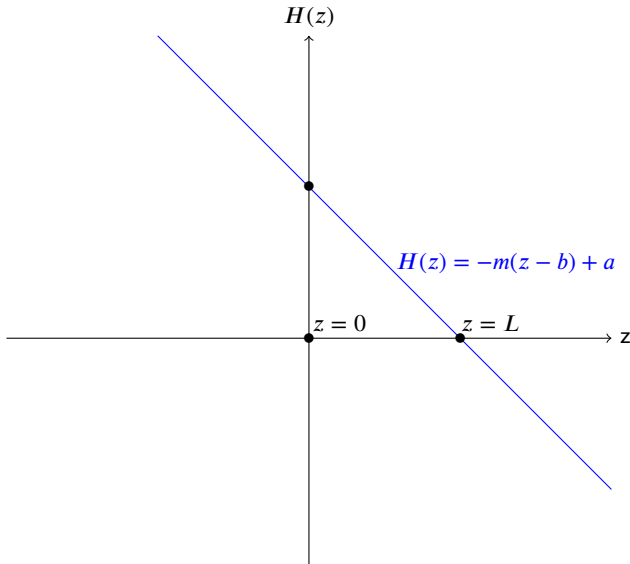

Figure 10: The linear distribution of the solute concentration in the fluid phase

As presented in Figure 10, the function H is defined as

$$H(z) = -m(z - b) + a \tag{113}$$

The function H can be integrated over the integral from a to b to describe the total amount of solute in the fluid phase (S) in that interval.

$$\int_a^b H(z)dz = S \tag{114}$$

If parameter a describe the beginning of the fixed bed, then $a = 0$. Similarly, b can be defined as the end of the fixed bed, then $b = L$. On range from $a = 0$ to $b = L$ the result of this integral is know, and it is equal to

$$S = m_{fluid}^0 = \int_{a=0}^{b=L} -m(x - L)\,dz \tag{115}$$

where m_{fluid}^0 is the total mass of solute in the fluid phase and N is the number of intervals between a and b. The right-hand side of the above equation can be evaluated

$$\int_{a=0}^{b=L} -m(x-L)\,dz = -m\left(\int_{a=0}^{b=L} z\,dz - \int_{a=0}^{b=L} L\,dz\right)$$
$$= -m\left(\frac{z^2}{2}\Big|_0^L - Lz\Big|_0^L\right)$$
$$= -m\left(\frac{L^2}{2} - L^2\right)$$
$$= m\frac{L^2}{2} \tag{116}$$

The parameter m can be obtained by equating the left-hand side of Equation 115 and the right-hand side of Equation 116

$$m_{fluid}^0 = m\frac{L^2}{2} \rightarrow m = \frac{2m_{fluid}^0}{L^2} \tag{117}$$

As can be seen from the above equation, the linearly distributed concentration of solute in the fluid phase can be fully determined if parameters a, b and m_{fluid}^0 are know. m_{fluid}^0 can be obtained from the total mass of the solute in the system at the initial time m_{total}^0 and the partition factor τ.

$$\tau = \frac{\text{total mass of solute in the fluid phase}}{\text{total mass of solute in the system}} = \frac{m_{fluid}^0}{m_{total}^0}$$

The initial conditions can be summarized as

$$c_f(t = 0, z) = H(z)$$
$$c_s(t = 0, z) = c_{s0}$$
$$h(t = 0, z) = h_0$$

A.7. Maximum Likelihood

Maximum likelihood estimation (MLE) is a statistical method used to estimate the parameters of a probability distribution based on observed data. The MLE works by finding the values of the parameters that maximize the likelihood function, which is the probability of observing the given data for a given set of parameter values. The MLE has desirable properties such as asymptotic efficiency and normality. Although the MLE has often been associated with the normal distribution for mathematical convenience, it can be applied to a wide range of probability distributions.

To find the maximum likelihood estimates, we maximize the joint probability density function, or likelihood function, denoted as $p(\theta|y(t_1), y(t_2), ..., y(t_n))$, where θ represents the parameters and $y(t_1), y(t_2), ..., y(t_n)$ represent the observed data. The conditions at the maximum can be refined by incorporating prior information. The posterior probability density function $p(\theta|y)$ can be expressed as the ratio of two probability densities (103) using the continuous variable analogue of Bayes' theorem (details in Appendix A.4).

In such a case the posteriori distribution is given by Equation 119.

$$p\left(\theta|y(t_n),...,y(t_1)\right) = \frac{p\left(\theta, y(t_n),...,y(t_1)\right)}{p\left(y(t_n),...,y(t_1)\right)} \tag{119}$$

The numerator of the right-hand side od Equation 119 using Equation 104a becomes

$$p\left(\theta, y(t_n),...,y(t_1)\right) = p\left(y(t_n)|\theta, y(t_{n-1}),...,y(t_1)\right) \\ \cdot p\left(\theta, y(t_{n-1}),...,y(t_1)\right) \tag{120}$$

These operations can be continued repetitively until we get

$$p\left(\theta, y(t_n),...,y(t_1)\right) = p(\theta)\prod_{i=1}^{n} p\left(y(t_i)|\theta, y(t_{i-1}),...,y(t_1)\right) \tag{121}$$

Examination of Equation 29 shows that $dY(t_i)/dt$ depends only on t_i, θ and $\epsilon(t_i)$ and is not conditioned by any previous measurement. Consequently, we can write

$$p\left(y(t_i)|\theta, y(t_{i-1}),...,y(t_1)\right) = p\left(y(t_i)|\theta\right) \tag{122}$$

provided Equation 29 is observed as a constraint. The desired joint conditional probability function is thus

$$p\left(\theta|y(t_n),...,y(t_1)\right) = \frac{p(\theta)\prod_{i=1}^{n} p\left(y(t_i)|\theta\right)}{p\left(y(t_n),...,y(t_1)\right)} \tag{123}$$

We can get rid of the evidence term $p\left(y(t_n),...,y(t_1)\right)$ because it's constant with respect to the maximization. Moreover, if we are lacking a prior distribution over the quantity we want to estimate, then $p(\theta)$ can be omitted. In such a case:

$$p\left(\theta|y(t_n),...,y(t_1)\right) = \prod_{i=1}^{n} p\left(y(t_i)|\theta\right) = \prod_{i=1}^{n} L\left(\theta|y(t_i)\right) \tag{124}$$

The likelihood function $L\left(\theta|y\right)$ for the parameters based on several observations is the product of the individual functions if the observations are independent.

$$L\left(\theta|y(t_n),...,y(t_1)\right) = \prod_{i=1}^{n} L\left(\theta|y(t_i)\right) \\ = p\left(y(t_1)|\theta\right) p\left(y(t_2)|\theta\right)...p\left(y(t_n)|\theta\right) \tag{125}$$

In choosing as estimates of θ the values that maximize L for the given values $\left(y(t_i)\right)$, it turns out that it is more convenient to work with the $\ln L$ than with L itself:

$$\ln L = \ln p\left(y(t_1)|\theta\right)+\ln p\left(y(t_2)|\theta\right)+...+\ln p\left(y(t_n)|\theta\right) = \sum_{i=1}^{n} \ln p\left(y(t_i); \theta\right) \tag{126}$$

By assuming that the conditional distribution of $\bar{Y}_i$, given y_i, is normal, then we form the likelihood function based on the probability density:

$$p\left(\theta, \sigma|y(t_n),...,y(t_1)\right) = \prod_{i=1}^{n} \frac{1}{\sqrt{2\pi}\sigma}\exp\left[\frac{1}{2\sigma}\left(Y(t_i)-y(\theta,t_i)\right)^2\right]$$

$$L\left(\theta, \sigma|y(t_n),...,y(t_1)\right) = \prod_{i=1}^{n} \frac{1}{\sqrt{2\pi}\sigma}\exp\left[\frac{1}{2\sigma}\left(Y(t_i)-y(\theta,t_i)\right)^2\right] \tag{127}$$

where σ is the variance

By taking the natural logarithm of the Equation 127, the final form of the objective function can be obtained:

$$\ln L = -\frac{n}{2}\left(\ln\sqrt{2\pi}+\ln\sigma^2\right) - \frac{\sum_{i=1}^{n}\left[Y(t_i)-y(\theta,t_i)\right]^2}{2\sigma^2} \tag{128}$$

RUN	VOLUME (cc)	DENSITY (g/cc)
	Run Data	
1	44.1311	1.2585
2	44.1423	1.2582
3	44.2163	1.2561
4	44.2709	1.2546
5	44.2365	1.2555

Figure 11: The result of solid density measurement

A.8. Solid density measurement

$$\rho_s^{ave} = \frac{1.2585 + 1.2582 + 1.2561 + 1.2546 + 1.2555}{5} = 1.25658[g/cc]$$

A.9. Porosity Calculations

To calculate the porosity of the solid particles ϕ, we can use the following formula:

$$\phi = \frac{\text{Volume with pores} - \text{Volume without pores}}{\text{Volume with pores}} \tag{129}$$

We can first calculate the volume, excluding the pore space, using the true density of the material:

$$\text{Volume excluding pores} = \frac{\text{mass}}{\text{true density}} = \frac{1\,\text{kg}}{1256.58\,\text{kg/m}^3} 0.0007958\,\text{m}^3 \tag{130}$$

We can then use the volume of the solid particles, including the pore space and the volume excluding the pore space, to calculate the porosity:

$$\phi = \frac{\text{Volume with pores} - \text{Volume without pores}}{\text{Volume with pores}} \tag{131}$$

Since 1 kg of solid particles occupies 1.6 L, which is equivalent to 0.0016 m³, we have:

$$\phi = \frac{0.0016 \text{ m}^3 - 0.0007958 \text{ m}^3}{0.0016 \text{ m}^3} = 0.5026 \qquad (132)$$

Therefore, the porosity of the solid particles is 0.5026 or 50.26%. This means that half of the total volume of the solid particles is made up of pore space.
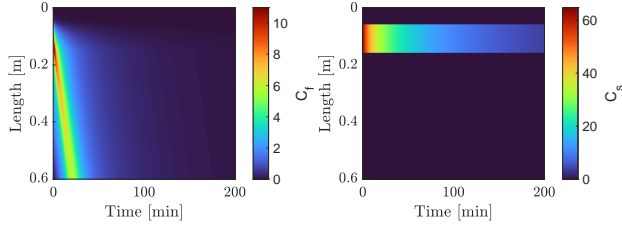
A.10. Concentration profiles

The time evolution of concentration profiles along the extractor for each dataset is presented on Figure 12. The concentration profiles use the parameters obtained from the parameter estimation. The plots on the left hand-side show the fluid phase concentration, while the plots on the right-hand side present the concentration in the solid phase.
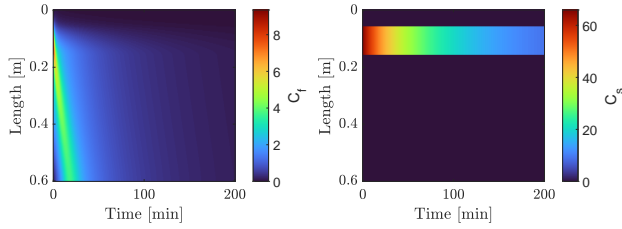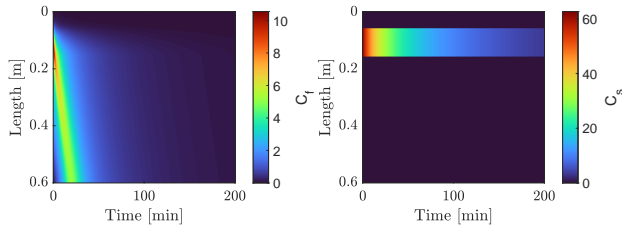
(a) Experiment at 40°C and 200 bar
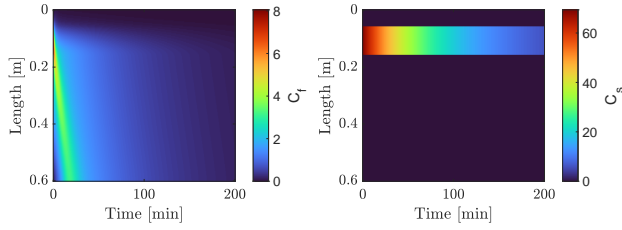
(b) Experiment at 50°C and 200 bar

(c) Experiment at 40°C and 300 bar

(d) Experiment at 50°C and 300 bar

Figure 12: Concentration profiles after solving the parameter estimation problem